DOT/FAA/TC-19/3

Federal Aviation Administration
William J. Hughes Technical Center
Aviation Research Division
Atlantic City International Airport
New Jersey 08405

Cyclic Plate Testing of Reinforced Airport Pavements—Phase I: Geogrid

February 2019

Final Report

U.S. Department of Transportation
Federal Aviation Administration

NOTICE

Technical Report Documentation Page

1. Report No.	2. Government Accession No.	3. Recipient=s Catalog No.
DOT/FAA/TC-19/3		

4. Title and Subtitle	5. Report Date
CYCLIC PLATE TESTING OF REINFORCED AIRPORT PAVEMENTS—PHASE I: GEOGRID	February 2019
	6. Performing Organization Code: USACE-ERDC
7. Author(s): Gregory J. Norwood	8. Performing Organization Report No.
9. Performing Organization Name and Address: U.S. Army Engineer Research and Development Center, Geotechnical and Structures Laboratory, 3909 Halls Ferry Road, Vicksburg, Mississippi 39180-6199	10. Work Unit No. (TRAIS)
	11. Contract or Grant No.
12. Sponsoring Agency Name and Address: U.S. Department of Transportation, Federal Aviation Administration, Air Traffic Organization Operations Planning, Office of Aviation Research and Development, Washington, DC 20591	13. Type of Report and Period Covered: Final Report
	14. Sponsoring Agency Code: AAS-100

15. Supplementary Notes
The Federal Aviation Administration Aviation Research Division COR was Mr. Jeffrey Gagnon.

16. Abstract
Numerous recent studies have examined pavement design using geosynthetics as a method to improve pavement performance in terms of reducing material thickness or increased pavement life. Most of this work has been focused on highway pavement design and loading scenarios. This study was examines the effect of using geosynthetics as a reinforcement agent in airfield pavement design with pavement structures subjected to heavy aircraft loadings. Cyclic plate testing was conducted on field-scale pavement layers within a laboratory pavement testing containment facility. Four representative weak airfield pavement structures were constructed, three of which included geogrid reinforcement at the bottom of the aggregate base-course layer. The pavement structures were constructed in similar fashion, which allows for comparison of pavement performance data between the test items. Pavement performance data were collected and examined. This data included permanent deformation of the pavement layers and stress distribution of the heavy aircraft loading. Traffic benefit ratios were calculated as a means to easily compare reinforced versus unreinforced pavement performance.

Test results concluded there is significant increase in pavement performance when using geogrid reinforcement in a weak airfield pavement structure. The traffic benefit ratios for all geogrid-reinforced test items showed substantial improvement and can be used as a basis for additional full-scale accelerated pavement testing.

17. Key Words	18. Distribution Statement
Geosynthetics, Cyclic plate testing, Pavement design, Traffic benefit ratio, Geogrid, Reinforcement, Flexible pavement	This document is available to the U.S. public through the National Technical Information Service (NTIS), Springfield, Virginia 22161. This document is also available from the Federal Aviation Administration William J. Hughes Technical Center at actlibrary.tc.faa.gov.

19. Security Classif. (of this report)	20. Security Classif. (of this page)	21. No. of Pages	22. Price
Unclassified	Unclassified	58	

TABLE OF CONTENTS

LIST OF FIGURES

LIST OF TABLES

LIST OF ACRONYMS

AASHTO	American Association of State Highway and Transportation Officials
AC	Asphalt content
ASTM	American Society of Testing and Materials
C_c	Coefficient of Conformity
C_u	Coefficient of Uniformity
CBR	California Bearing Ratio
CH	High-plasticity clay
DCP	Dynamic cone penetrometer
EPC	Earth pressure cell
ERDC	U.S. Army Engineer Research and Development Center
FAA	Federal Aviation Administration
G_{mb}	Bulk specific gravity
G_{mm}	Theoretical maximum specific gravity
G_{sb}	Bulk (dry) specific gravity
GP-GM	Poorly graded gravel with silt and sand
HMA	Hot-mix asphalt
HT	High type
kN/m	Kilo-Newton per meter
LL	Liquid limit
LVDT	Linear variable displacement transducers
MDOT	Mississippi Department of Transportation
MTC	Materials Testing Center (ERDC)
NAT W%	Water content
NP	Nonplastic
pcf	Pounds per cubic foot
PG	Performance grade
PI	Plasticity index
PL	Plastic limit
psi	Pounds per square inch
SP	Poorly graded sand
Sp. G.	Specific gravity
TBR	Traffic benefit ratio
USCS	Unified Soil Classification System
VFA	Voids filled with asphalt
VMA	Voids in mineral aggregate
ZAV	Zero air voids

EXECUTIVE SUMMARY

Numerous recent studies have examined pavement design using geosynthetics as a method to improve pavement performance in terms of reducing material thickness or increased pavement life. Most of this work has been focused on highway pavement design and loading scenarios. This study examines the effect of using geosynthetics as a reinforcement agent in airfield pavement design with pavement structures subjected to heavy aircraft loadings. Cyclic plate testing was conducted on field-scale pavement layers within a laboratory pavement testing containment facility. Four representative weak airfield pavement structures were constructed, three of which included geogrid reinforcement at the bottom of the aggregate base-course layer. The pavement structures were constructed in similar fashion, which allows for comparison of pavement performance data between the test items. Pavement performance data collected and examined included permanent deformation of the pavement layers and stress distribution of the heavy aircraft loading. Traffic benefit ratios were calculated as a means to easily compare reinforced versus unreinforced pavement performance.

Test results concluded there is significant increase in pavement performance when using geogrid reinforcement in a weak airfield pavement structure. The traffic benefit ratios for all geogrid-reinforced test items showed substantial improvement and can be used as a basis for additional full-scale accelerated pavement testing.

1. INTRODUCTION.

Geosynthetics have been used in highway pavement applications for years. Recently, pavement design engineers have proposed using geosynthetics in airfield pavement design. The Federal Aviation Administration (FAA) is interested in determining the merit of using geosynthetics as a structural element in flexible airfield pavement design and the benefits gained from doing so. Geogrid reinforcement is the main geosynthetic product that historically has been implemented as a mechanism for reducing pavement thickness or increasing pavement life. Testing of these pavement systems traditionally has been performed in the form of construction and traffic testing of full-scale pavement test sections. These tests tend to be costly and time consuming in terms of both construction and testing. Pavement structures constructed in a laboratory box-testing containment facility provide an excellent opportunity to quantify benefits of geogrid reinforcement at a reduced cost to full-scale traffic testing.

The technical objective of this effort is to conduct medium-scale laboratory testing of representative flexible airfield pavements including different types of geosynthetic reinforcement. These different products and methods were compared to one another, as well as an unreinforced control test, based on pavement performance under simulated aircraft loadings. Pavement performance was measured by accumulated rut depth, which was used to calculate a traffic benefit ratio (TBR) for each product tested. To determine the TBR, four test items were constructed in a 6-ft square laboratory box-testing facility. Each test item consisted of the same pavement structure with a different geogrid placed at the base-subbase interface. Earth- and pore-pressure sensors were embedded in the subgrade of the various test items, and displacement sensors were placed at the pavement surface. Testing was accomplished via cyclic loading of a 12-in.-diameter, circular plate at the surface of the pavement section. Response data were collected during cyclic loading. Data collected included deformation at the pavement surface, deformation under the load plate, vertical pressure in the subgrade, and pore pressures in the subgrade.

2. MATERIALS.

Materials used during construction of the laboratory test items are described in sections 2.1 through 2.5. Subgrade, subbase, base, and surface layer materials underwent a suite of laboratory characterization tests prior to construction of the laboratory box-test items. The test results are summarized in sections 2.1 through 2.5.

2.1 SUBGRADE.

The subgrade was constructed using locally available clay, known as Vicksburg Buckshot Clay. This soil has been used in historical full-scale pavement testing at the U.S. Army Engineer Research and Development Center (ERDC). Figure 1 shows the grain size distribution chart for the Buckshot Clay used in this test series. The soil is composed of 98.6% fines passing the No. 200 sieve. The liquid limit (LL), plastic limit (PL), and plastic index (PI) were 90, 28, and 62, respectively. The soil classifies as a high-plasticity clay (CH) in the Unified Soil Classification System (USCS) [1] and A-7-6(63) according the American Association of State Highway and Transportation Officials (AASHTO) procedure [2 and 3]. Modified Proctor tests were performed in accordance with ASTM D1557, Method C [4]. The results of this test are

shown in figure 2. At the target moisture content of 19.8%, the maximum dry density of the subgrade material is 101.4 pounds per cubic foot (pcf).

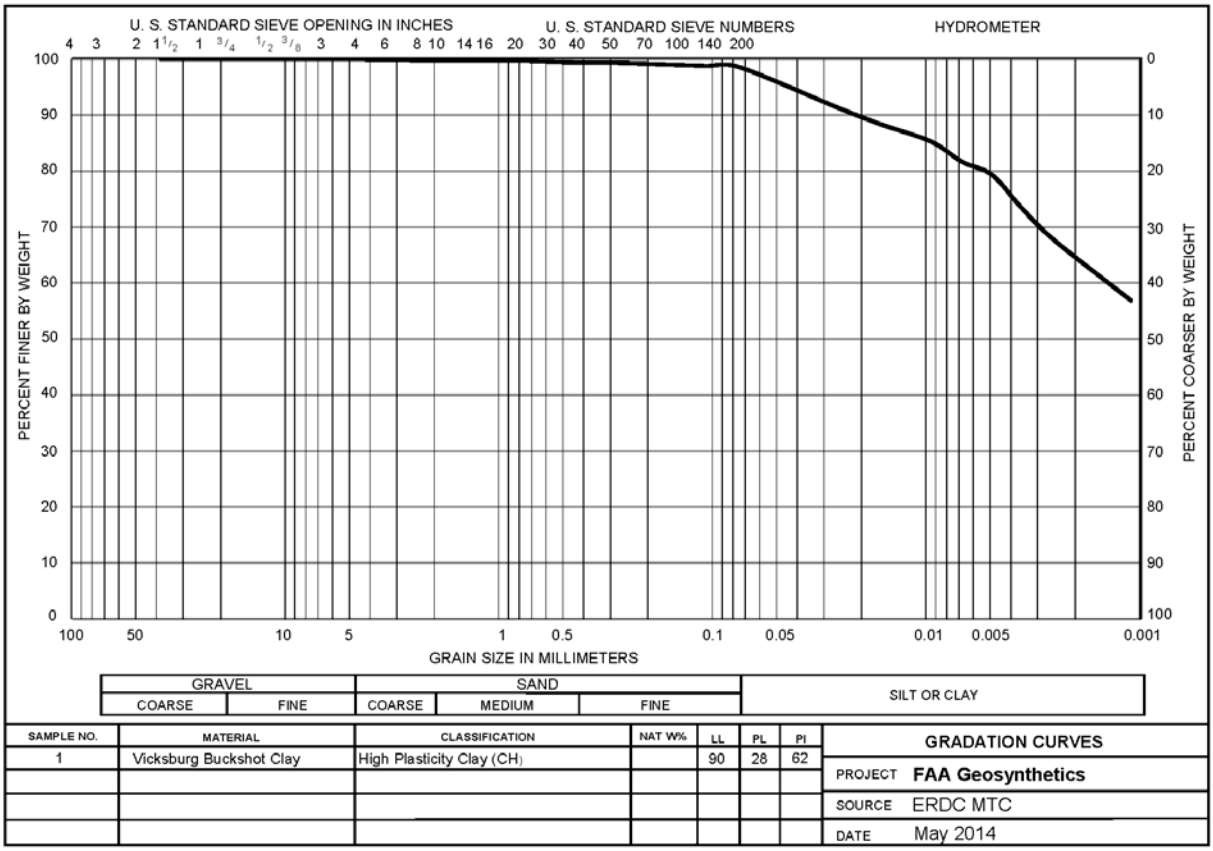

NAT W% = Natural moisture content
MTC = Materials Testing Center

Figure 1. Gradation for Subgrade Material

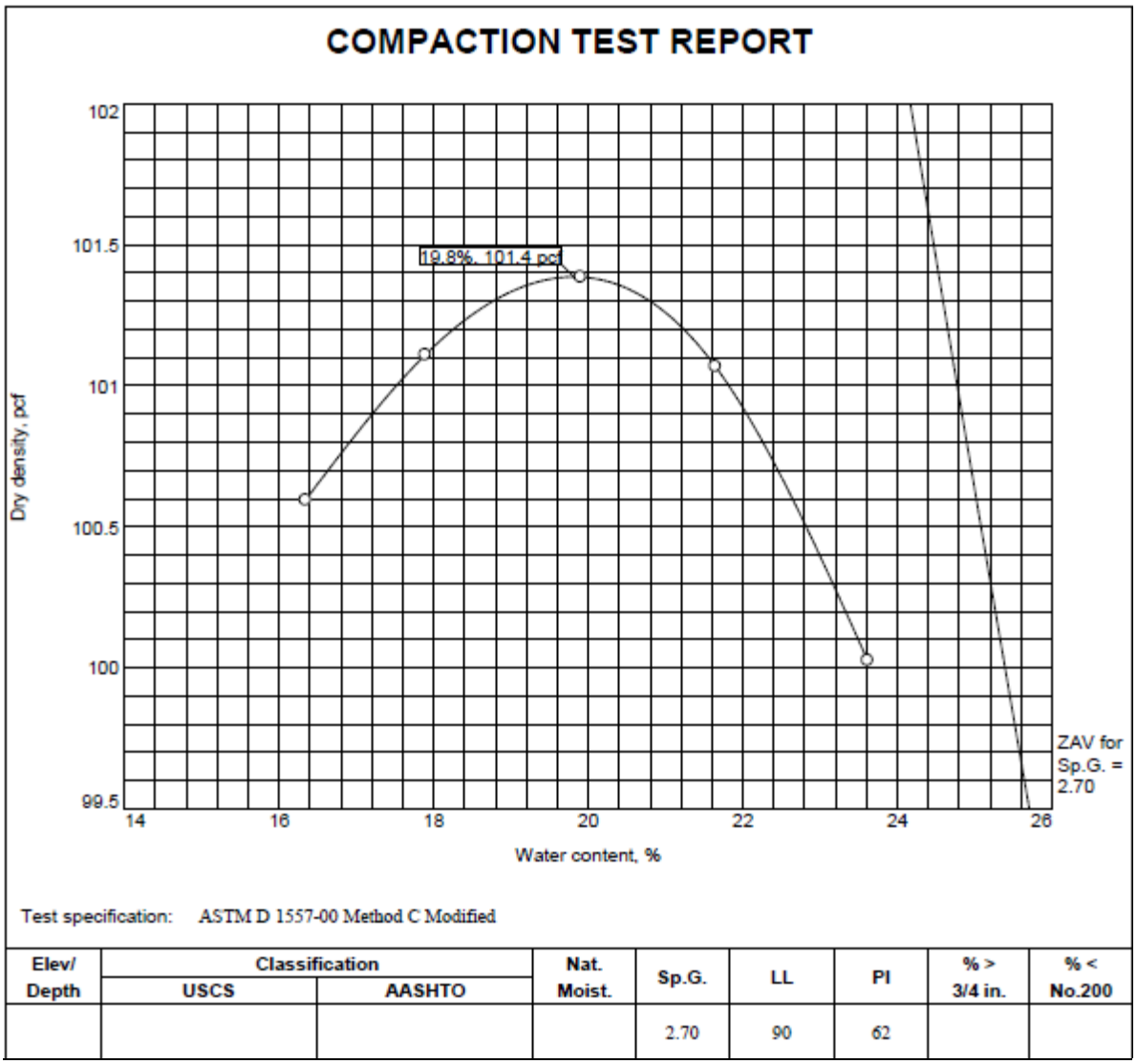

Elev/ Depth	Classification		Nat. Moist.	Sp.G.	LL	PI	% > 3/4 in.	% < No.200
	USCS	AASHTO						
				2.70	90	62		

ZAV = Zero air voids
Sp.G. = Specific gravity
Nat. Moist. = Natural moisture content

Figure 2. Compaction Test Results for CH Subgrade

2.2 SUBBASE.

The subbase was constructed using a locally available granular material that met the gradation requirements for FAA P-154 material. The grain size distribution chart for the subbase material is shown in figure 3. The ASTM D2487 procedure [1] was used to determine the subbase material was comprised of 1.6% gravel, 98.4% sand, and 0% fines passing the No. 200 sieve. The coefficient of curvature (C_c) was calculated as 0.40, and the coefficient of uniformity (C_u) was 2.89. The subbase material was classified as a poorly graded sand (SP) according to the USCS and an A-1-b according to the AASHTO procedure [2]. Requirements for FAA P-154 subbase material are presented in table 1 along with the gradation of the placed subbase material used during testing.

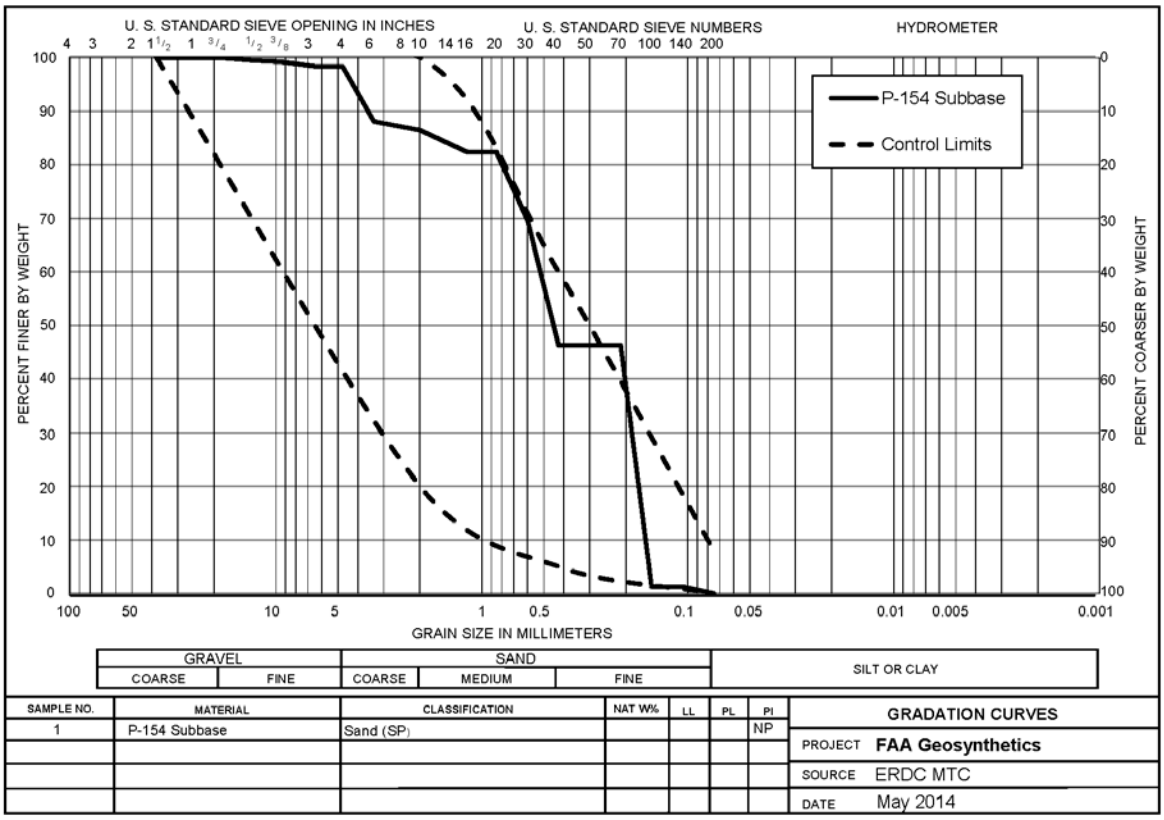

NP = Nonplastic

Figure 3. Gradation for P-154 Subbase Material

Table 1. The FAA P-154 Gradation Requirements

Sieve	FAA % Passing Requirements	Subbase Material % Passing
3 in. (75.0 mm)	100	100
No. 10 (2.0 mm)	20-100	86.5
No. 40 (0.450 mm)	5-60	46.3
No. 200 (0.075 mm)	0-8	0.2

Notes: The portion of the material passing the No. 40 (0.450 mm) sieve shall have a liquid limit of not more than 25 and a plasticity index of not more than 6 when tested in accordance with ASTM D4318 [5].
The maximum amount of material finer than 0.02 mm in diameter shall be less than 3% [5].

2.3 BASE COURSE.

The base course was constructed using a locally available 610 crushed limestone material. The grain size distribution chart for the crushed limestone is shown in figure 4. The ASTM D2487 procedure [1] was used to determine that the base course was comprised of 46.4% gravel, 43.6%

sand, and 10.0% nonplastic fines passing the No. 200 sieve. The C_c was calculated as 9.08, and the C_u was 80.09. The crushed limestone aggregate base was classified as a poorly graded gravel with silt and sand (GP-GM) according to the USCS [1], and an A-1-a according to the AASHTO procedure [2]. Requirements for FAA P-209 base material are presented in table 2 along with the gradation of the placed base-course material used during testing. Modified Proctor compaction tests were performed in accordance with ASTM D1557 Method C [4]. The maximum dry density was 144.7 pcf at an optimum moisture content of 4.9%.

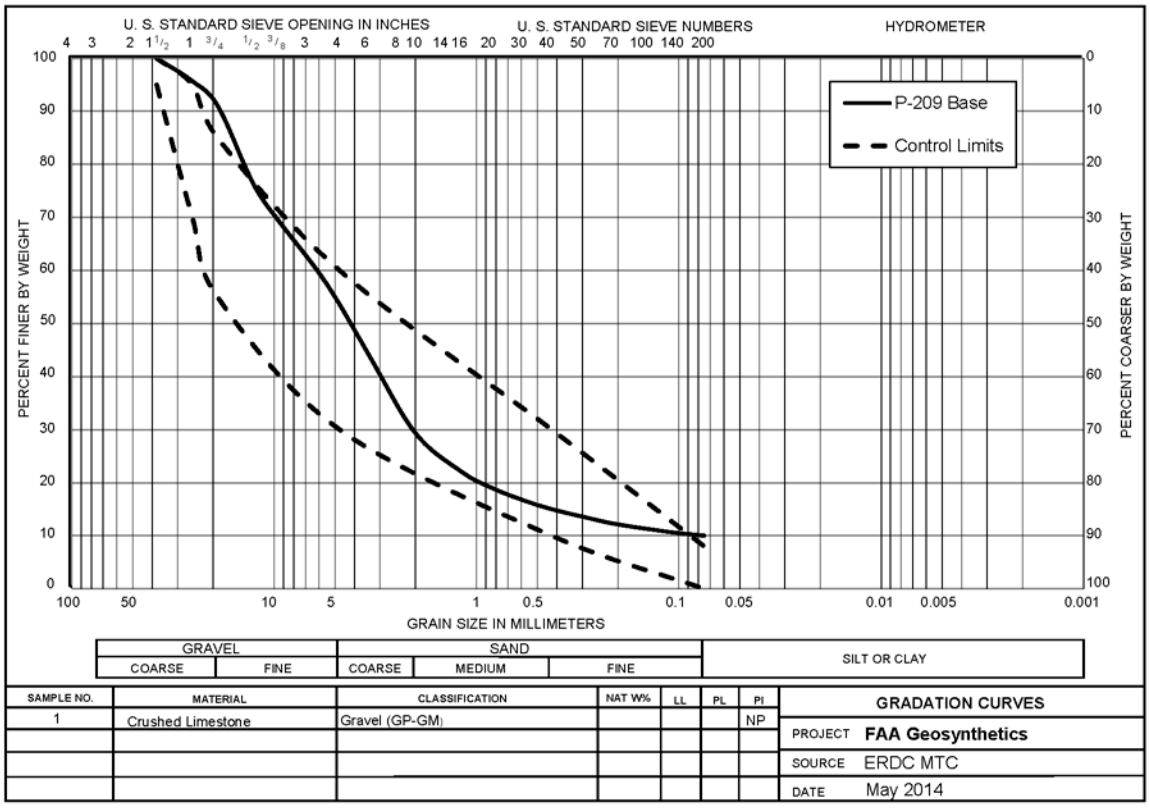

Figure 4. Gradation for P-209 Base Material

Table 2. Base Course Gradation Requirements

Sieve Size	FAA P-209 % Passing Requirements	Job Mix Tolerances %	610 Crushed Limestone % Passing
2 in. (50.0 mm)	100	0	100
1-1/2 (37.0 mm)	95-100	±5	100
1 in. (25.0 mm)	70-95	±8	96
3/4 in. (19.0 mm)	55-85	±8	91
No. 4 (4.75 mm)	30-60	±8	54
No. 30 (0.60 mm)	12-30	±5	17
No. 200 (0.075 mm)	0-5	±3	10

2.4 HOT-MIX ASPHALT.

The surface course for each test item was constructed using a locally available Mississippi Department of Transportation (MDOT) 12.5-mm high type (HT) mix with a PG 67-22 binder. A comparison of the mix design and FAA requirements for P-401 are shown in table 3. As-constructed hot-mix asphalt (HMA) properties are discussed in section 4.6.

Table 3. The HMA Gradation Comparison

Sieve	FAA P-401 Gradations				HMA Job Mix Formula
	1-1/2 in. Maximum	1 in. Maximum	3/4 in. Maximum	1/2 in. Maximum	
1-1/2 in. (37.5 mm)	100	--	--	--	100
1 in. (24.0 mm)	86-98	100	--	--	100
3/4 in. (19.0 mm)	68-93	76-98	100	--	100
1/2 in. (12.5 mm)	57-81	66-86	79-99	100	97
3/8 in. (9.5 mm)	49-69	57-77	68-88	79-99	86
No. 4 (4.75 mm)	34-54	40-60	48-68	58-78	55
No. 8 (2.36 mm)	22-42	26-46	33-53	39-59	37
No. 16 (1.18 mm)	13-33	17-37	20-40	26-46	26
No. 30 (0.600 mm)	8-24	11-27	14-30	19-35	20
No. 50 (0.300 mm)	6-18	7-19	9-21	12-24	13
No. 100 (0.150 mm)	4-12	6-16	6-16	7-17	8
No. 200 (0.075 mm)	3-6	3-6	3-6	3-6	5

2.5 GEOGRID.

Three geogrids were tested during this suite of tests: Tensar® TriAx® TX140 (figure 5), Tensar Biaxial BX1200 (figure 6), and HUESKER Fornit® 30/30 (figure 7). The TX140 is a triaxial geogrid consisting of a series of concentric triangles, forming a series of concentric hexagons. The BX1200 is a biaxial punched and drawn polypropylene geogrid consisting of a series of rectangles, providing reinforcement in the longitudinal and transverse directions. The Fornit 30/30 is comprised of polypropylene yarns manufactured with an interlocking pattern and then coated with a polymer. Material characteristics related to the products are summarized in table 4. Minimum rib thickness and tensile strength requirements are specified in ASTM D6637 [6].

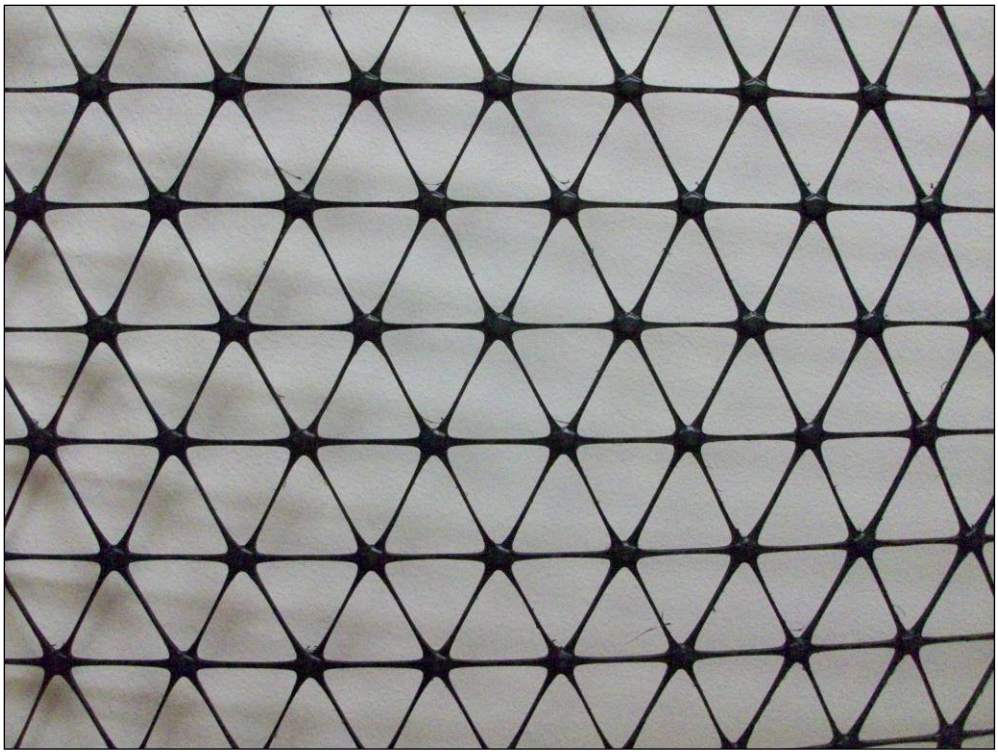

Figure 5. Tensar TX140

Figure 6. Tensar BX1200

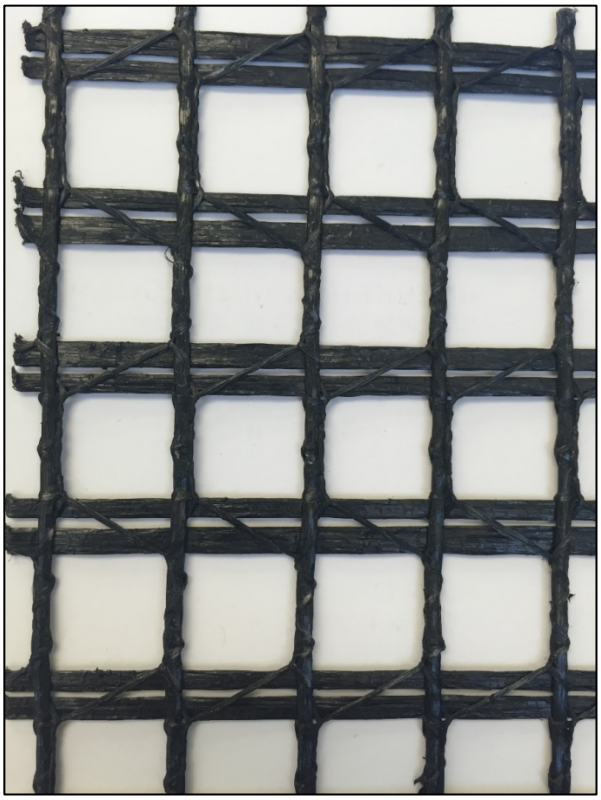

Figure 7. HUESKER Fornit 30/30

Table 4. Geogrid Material Characteristics

Product Index Properties	Units	BX1200		TX140	Fornit 30/30	
		Machine Direction Values	Cross Machine Direction Values	Not Available	Machine Direction Values	Cross Machine Direction Values
Aperture Dimensions	mm (in.)	25 (1.0)	33 (1.3)	Not Available	15 (0.6)	15 (0.6)
Minimum Rib Thickness (ASTM D6637 [6])	mm (in.)	1.27 (0.05)	1.27 (0.05)	Not Available	Not Available	Not Available
Tensile Strength at 2% Strain [6]	kN/m (lb/ft)	6.0 (410)	9.0 (620)	Not Available	8 (548)	13 (890)
Tensile Strength at 5% Strain [6]	kN/m (lb/ft)	11.8 (810)	19.6 (1340)	Not Available	20 (1370)	27 (1850)
Ultimate Tensile Strength [6]	kN/m (lb/ft)	19.2 (1310)	28.8 (1970)	Not Available	27 (1850)	35 (2398)

kN/m = Kilo-Newton per meter

3. TEST PLAN AND LAYOUT.

The following section details the overall plan for constructing and testing of the geogrid-reinforced laboratory box testing. The primary objective of this project was to quantify the performance of a representative geogrid-reinforced airport flexible pavement under simulated heavy aircraft loading. The approach was to build large-scale laboratory tests, each with a unique geogrid, and observe pavement performance under a series of loading conditions simulating shakedown. Response data in the pavement section were also obtained.

The test series consisted of four different test items. Figure 8 depicts the profile view of a typical test item constructed for this study. The test items were constructed in a 6-foot-square laboratory containment facility. Each test item was constructed with approximately 28 in. of high-plasticity clay as the subgrade material. The subgrade was overlain with a 12-in.-thick subbase course consisting of poorly graded granular material meeting FAA P-154 specifications [7]. A 7-in. base course of crushed limestone was placed on top of the subbase. The surface layer was a 5-in.-thick HMA slab. Overall thickness of each test section was approximately 52 in. Item 1 was the control section, which was constructed without any reinforcement. Item 2 was constructed using TX140 geogrid at the base-subbase interface. Item 3 was constructed using BX1200 geogrid at the base-subbase interface. Item 4 was constructed with Fornit 30/30 geogrid at the base-subbase interface.

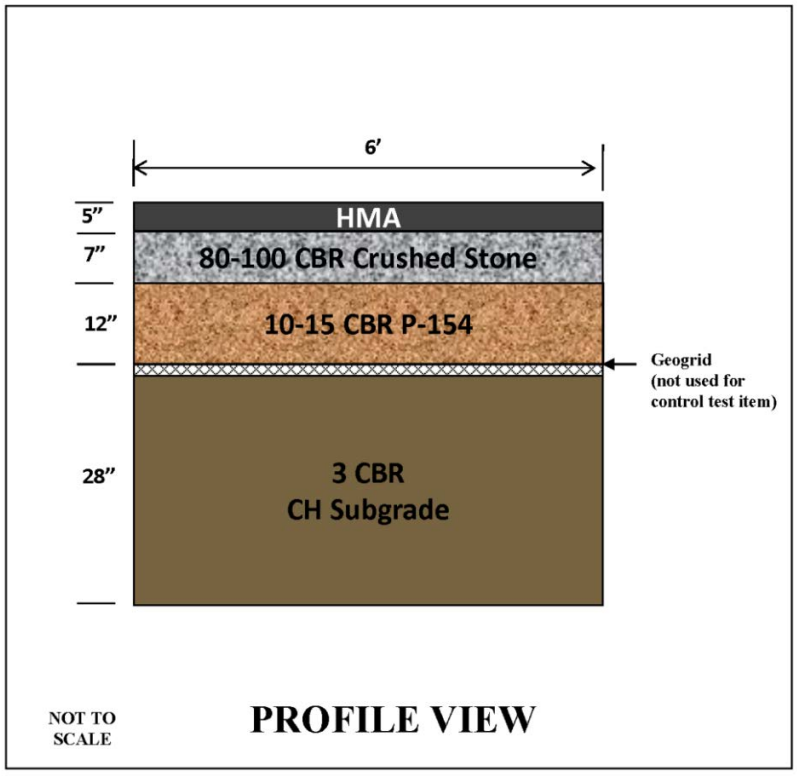

Figure 8. Profile View of a Typical Test Item

The high-plasticity clay subgrade materials and crushed limestone base materials underwent laboratory testing for characterization. Laboratory tests were performed to ensure that the materials were constructed at the appropriate moisture content and density to obtain the desired strength properties in the laboratory box-testing facility.

Instrumentation was placed at several locations within the pavement structure to obtain pavement response parameters. Response parameters of interest included deflections, stress, and strains at various locations in the pavement structure. Vertical stress was measured just below the base-subbase interface, just below the subbase-subgrade interface, and at a depth of approximately 26 in. below the subbase-subgrade interface. Elastic deflections and permanent deformations were measured along the centerline at the pavement surface. The loading actuator also contained a linear variable displacement transducer (LVDT) that was used to measure vertical deflections during testing. Finally, pore pressures and temperature were measured near the top of the subgrade during the construction, testing, and post-test phases. A profile view of the sensor layout is depicted schematically in figure 9. Note that all instrumentation installation depths in figure 9 are approximations intended to illustrate a typical test item. Final earth pressure cell (EPC) installation depths are discussed in section 4.7.1.

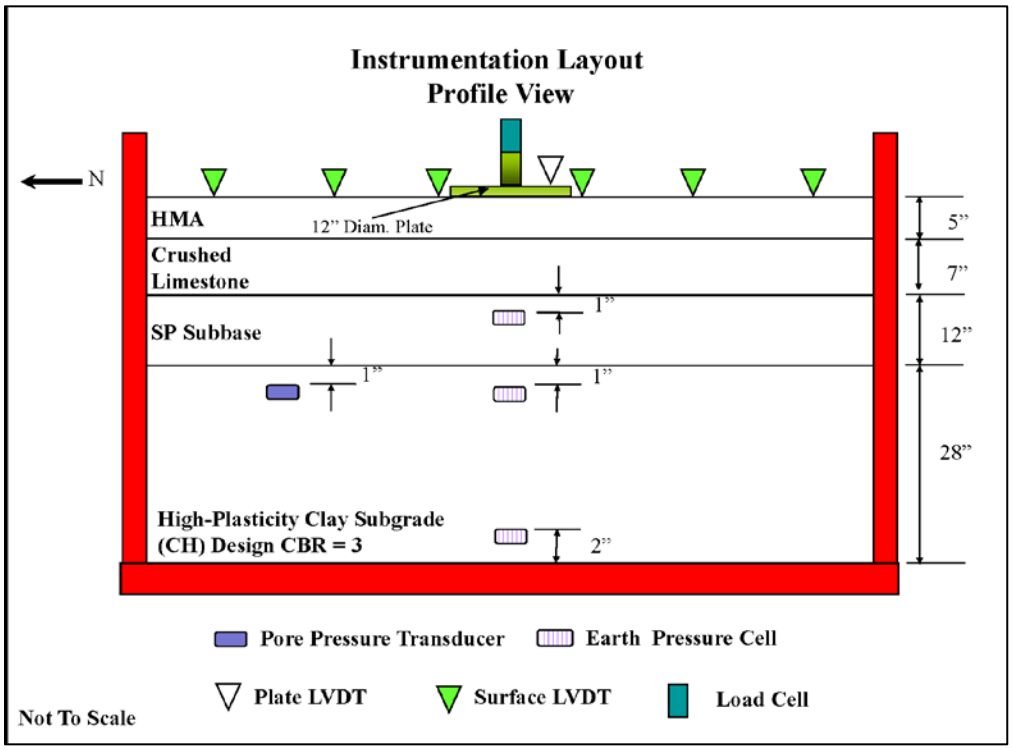

Figure 9. Pavement Sensors for a Typical Test Item, Profile View

After construction, the test items were loaded to failure via cyclic loading of a 12-in.-diameter plate. Loading was applied using a 1.2-second pulse. The load was applied with 0.3 seconds of loading followed by a 0.9-second rest period. A load of approximately 28,800 lb was applied to achieve the targeted 254 psi pavement loading. Testing was conducted until each test item registered greater than 2-in. permanent surface deformation beneath the loading plate. After

testing, forensic investigations were performed. Data collected during this phase included surface profiles and strength characterization at the base and subgrade surface.

4. CONSTRUCTION.

The test items were constructed and tested from March to December 2014. The construction procedures are documented in this section. Additionally, quality assurance data obtained during construction is summarized in this section.

4.1 LABORATORY BOX-TESTING FACILITY.

A 6-ft-square, 4.5-ft-deep, reinforced steel box was used as a containment facility for laboratory pavement structures. The box-testing facility was composed of 1-in.-thick steel plates reinforced with 1/4-in.-thick, 6-in.-square, structural steel tubing along the bottom and three sides of the box. The front of the facility was composed of removable 1/4-in.-thick, 6-in.-square structural steel tubing. The front of the facility was removed to aid in the construction process. The tubes were bolted to the containment facility one layer at a time as construction proceeded, simplifying the process of placing and compacting the soil materials within the test facility.

Prior to placement of the soil, the containment facility was lined with polyethylene to minimize moisture migration and desiccation of the test items during construction and testing. Figure 10 shows the lined box facility before placement of soil materials.

Figure 10. Lined Box-Testing Facility

4.2 SUBGRADE CONSTRUCTION.

The subgrade materials were spread out in a 12-in.-thick lift on a soil-processing strip. Subgrade soils were allowed to dry until reaching the desired moisture content. The soil was periodically pulverized using a rotary mixer, as shown in figure 11. The clay was mixed and pulverized in an iterative manner to break down the larger clay pieces and bring about moisture equilibrium. Upon reaching the desired moisture content, the clay was hand spread in the containment facility in thin lifts. Each lift was compacted using a pneumatic compactor, as shown in figure 12. Lift thicknesses were monitored and controlled by using a rod and level to take elevation readings during construction, as shown in figure 13. The readings were taken at the same locations for all pavement layers and test items. Figure 14 depicts the exact locations where the rod and level measurements were taken during construction for each pavement layer of each test item. The summarized average thickness data for all constructed layers are shown in table 5.

Figure 11. The CH Material Processing

Figure 12. Compaction of Subgrade Material

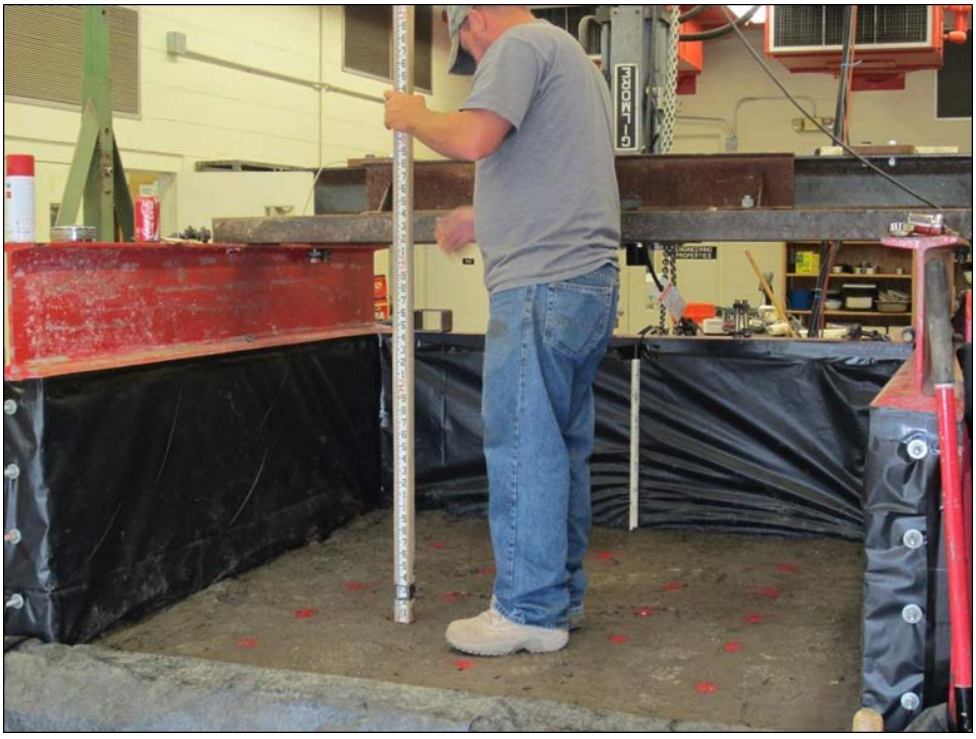

Figure 13. Thickness Control of Pavement Layers

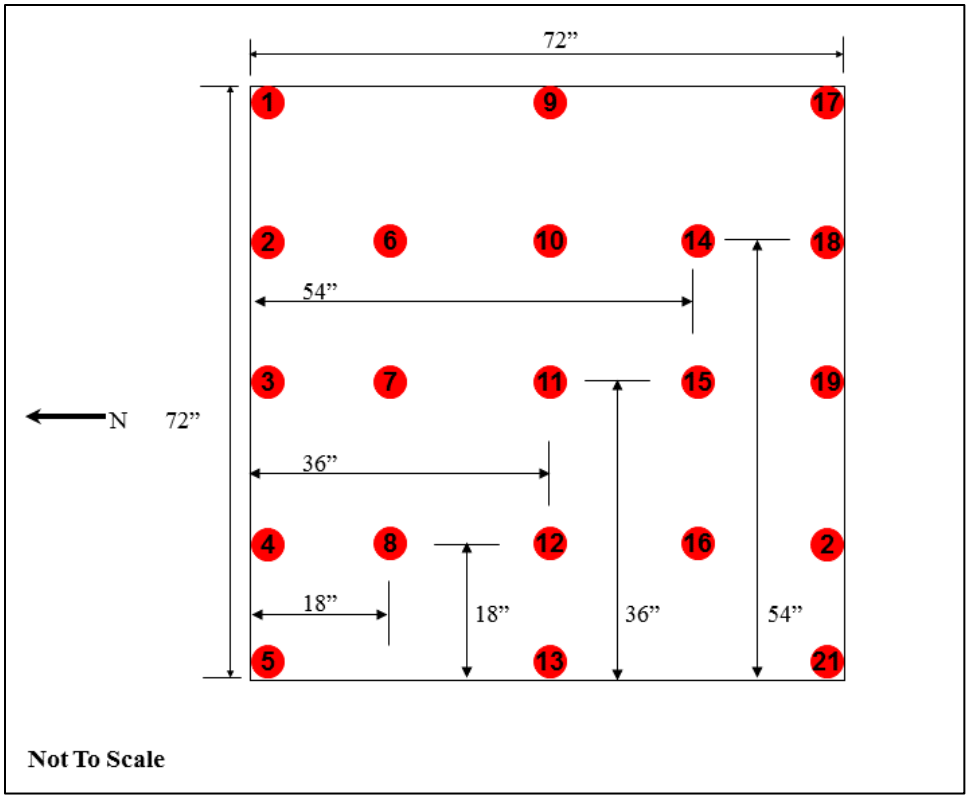

Figure 14. Thickness Control Survey Locations, Plan View

Table 5. Final Constructed Layer Thickness

Layer Thicknesses (in.)				
Layer	Control	TX140	BX1200	Fornit 30/30
HMA	4.8	5.0	5.1	5.1
Base	7.1	6.0	6.7	6.7
Subbase	12.2	12.4	12.3	12.4
Subgrade	27.8	28.9	28.4	28.0

Upon compaction of each subgrade lift, a series of tests were performed to ensure (a) the uniformity of the lift, and (b) the subgrade met the targeted strength of 3 California Bearing Ratio (CBR).

A nuclear densometer was used to obtain a measure of the moisture content and dry density. Samples were also taken to obtain oven-dried moisture contents. The results for all test items are summarized in table 6.

Table 6. Summary of As-Built Moisture, Density, and Strength Properties of the Subgrade

Product	Wet Density (pcf)	Dry Density (pcf)	Moisture Content (%)	Oven-Dried Moisture Content (%)
Control	110.3	83.1	32.7	35.4
TX140	112.9	84.7	33.4	38.3
BX1200	113.5	85.8	32.6	36.9
Fornit 30/30	114.3	86.2	32.5	36.8

Dynamic cone penetrometer (DCP) tests were performed upon compaction of the subgrade layers for each test section. The results from the DCP tests were used to verify constructed subgrade consistency and validated the subgrade strength. Results from DCP tests performed after each test item was fully constructed are presented later in section 4.5. In-field CBR tests were performed at the subgrade surface according to ASTM D4429 [8], as shown in figure 15. Post-construction CBR values are summarized in table 7.

Figure 15. The CBR Testing on the CH Subgrade

Table 7. Summary of Post-Construction Subgrade CBR Strengths

Test	Subgrade Surface CBR (%)
Control	3.6
TX140	3.4
BX1200	3.2
Fornit 30/30	3.1

4.3 SUBBASE CONSTRUCTION.

The granular subbase material was placed using a skid-steer loader, figure 16, and spread by hand over the subgrade in the testing box to the desired thickness. Each lift was compacted using a vibratory plate compactor, as shown in figure 17. After compaction, each lift was surveyed with a rod and level to ensure the targeted lift thickness was obtained. Figure 18 shows the survey points of the compacted and leveled subbase material surface. The thickness data for each test item is summarized in table 5. These thicknesses are average thicknesses from survey data obtained at the surface of the subgrade, subbase and base layers.

Upon compaction of the subbase layer, nuclear densometer readings were taken to characterize the in-place material properties. Samples were also taken to obtain oven-dried moisture contents. The results for all test items are summarized in table 8.

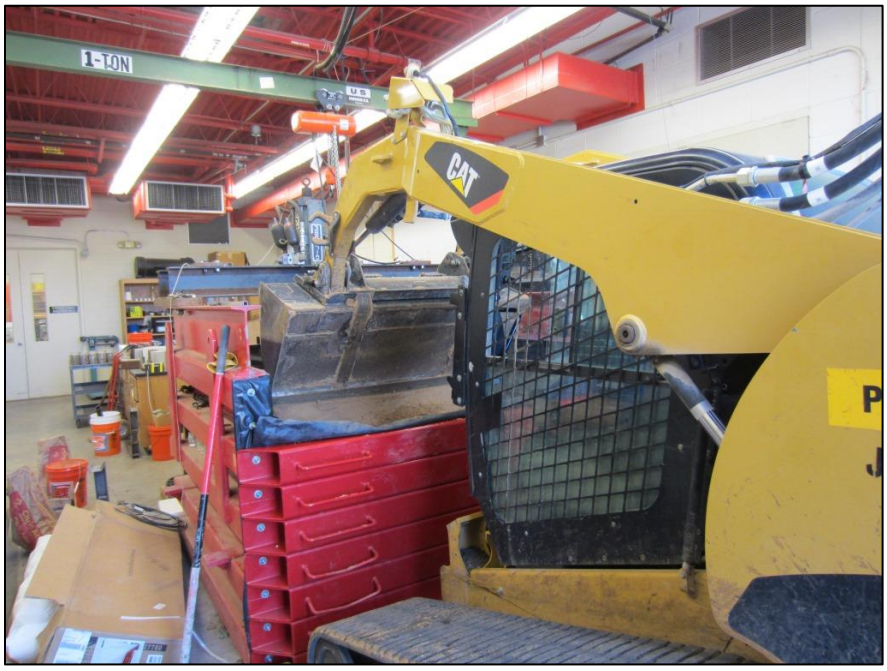

Figure 16. Subbase Material Placement

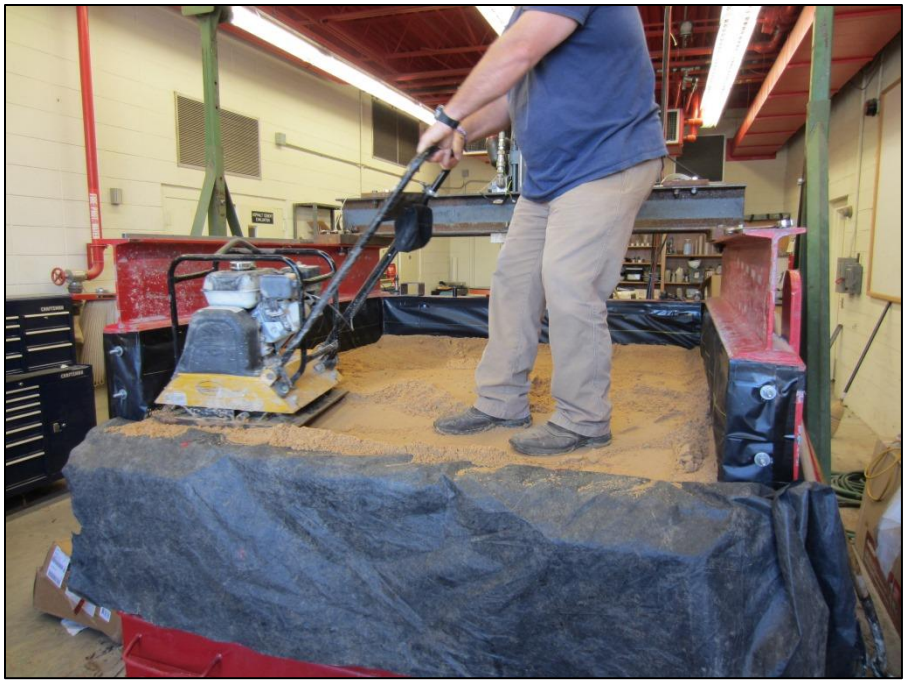

Figure 17. Compaction of Subbase Material

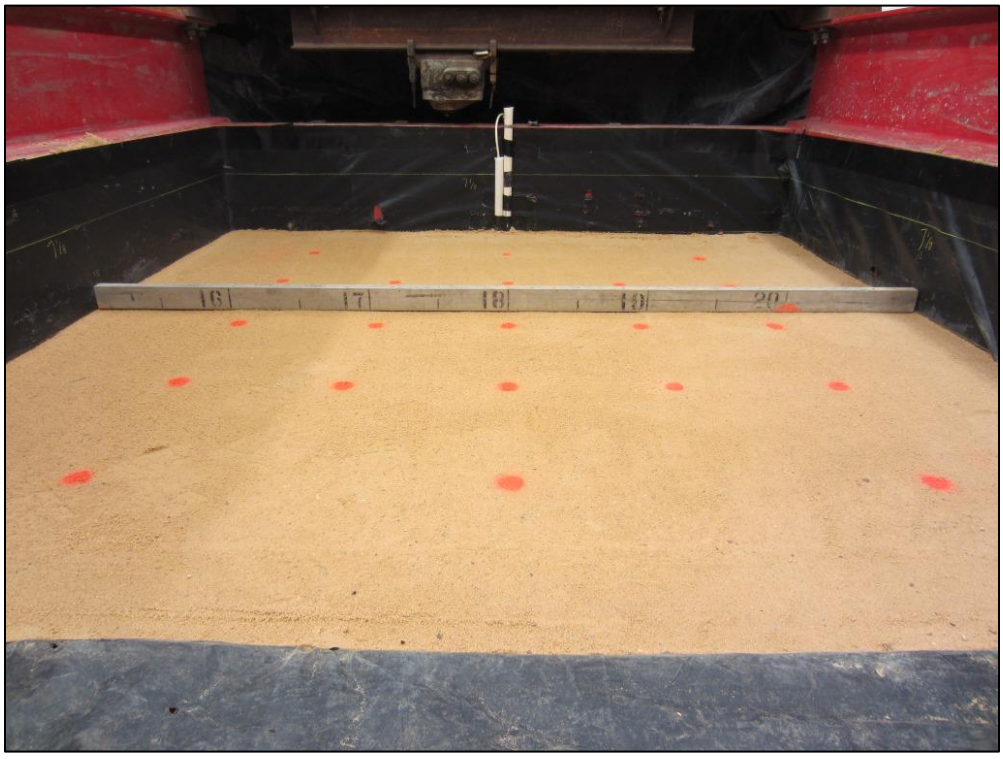

Figure18. Location of Survey Points on Subbase Surface

Table 8. Summary of As-Built Moisture, Density, and Strength Properties of the Subbase

Product	Wet Density (pcf)	Dry Density (pcf)	Moisture Content (%)	Oven-Dried Moisture Content (%)
Control	115.5	110.1	4.9	5.8
TX140	113.4	108.5	4.5	5.8
BX1200	112.9	109.4	3.2	5.9
Fornit 30/30	113.6	109.7	3.6	4.2

4.4 GEOGRID INSTALLATION.

For each test item, the appropriate geogrid was trimmed to the required dimensions for placement in the test box. The geogrid was pulled taught to prevent kinking during placement. Figure 19 shows the subgrade and geogrid surface prior to placement of the crushed limestone base.

Figure 19. Prepared Surface Prior to Placement of Crushed Limestone Materials

4.5 BASE-COURSE CONSTRUCTION.

The 610 crushed limestone aggregate was placed using a skid-steer loader, figure 20, and spread by hand over the geogrid surface in the testing box to the desired thickness. Each lift was compacted using a vibratory plate compactor, as shown in figure 21. After compaction, each lift was surveyed with a rod and level to ensure the targeted lift thickness was obtained. The thickness data for each test item are summarized in table 5. These are average thicknesses from survey data obtained at the surface of the subgrade, subbase, and base layers.

Figure 20. Placement of Base-Course Material

Figure 21. Compaction of the Aggregate Base Course Using Vibratory Plate Compactor

Upon compaction of the base course, a series of tests were performed on the limestone to ensure (a) the uniformity of the lift and (b) the strength of the unbound aggregate lift.

A nuclear densometer was used to obtain a measure of the moisture content and dry density. Samples were also taken to obtain oven- and microwave-dried moisture contents. These results are summarized in table 9.

Table 9. Summary of As-Built Moisture, Density, and Strength Properties of the Base Course

Product	Wet Density (pcf)	Dry Density (pcf)	Moisture Content (%)	Oven-Dried Moisture Content (%)
Control	141.4	134.3	5.3	5.1
TX140	140.2	137.9	1.7	4.8
BX1200	139.2	136.4	2.1	5.1
Fornit 30/30	140.2	137.9	1.7	4.8

DCP tests were performed after compaction of the base course, as shown in figure 22. The U.S. Army Corps of Engineers Dual-Mass DCP was used. The large (17.6 lb) hammer was use at the surface, and the small (10.1 lb) hammer was used in the subgrade zone. Raw data was analyzed using Webster's general equation relating DCP Index (mm/blow) to CBR strength (%) [9 and 10]. The DCP data are shown in figures 23 through 26 for items 1, 2, 3, and 4, respectively. These DCP results incorporate all pavement layers excluding the surface HMA layer. The interface between the different layers is clearly defined in the DCP results. In-field CBR tests were performed at the base surface according to ASTM D4429 [8]. Post-construction CBR values are summarized in table 10.

Figure 22. The DCP Testing at the Surface of the Base Course

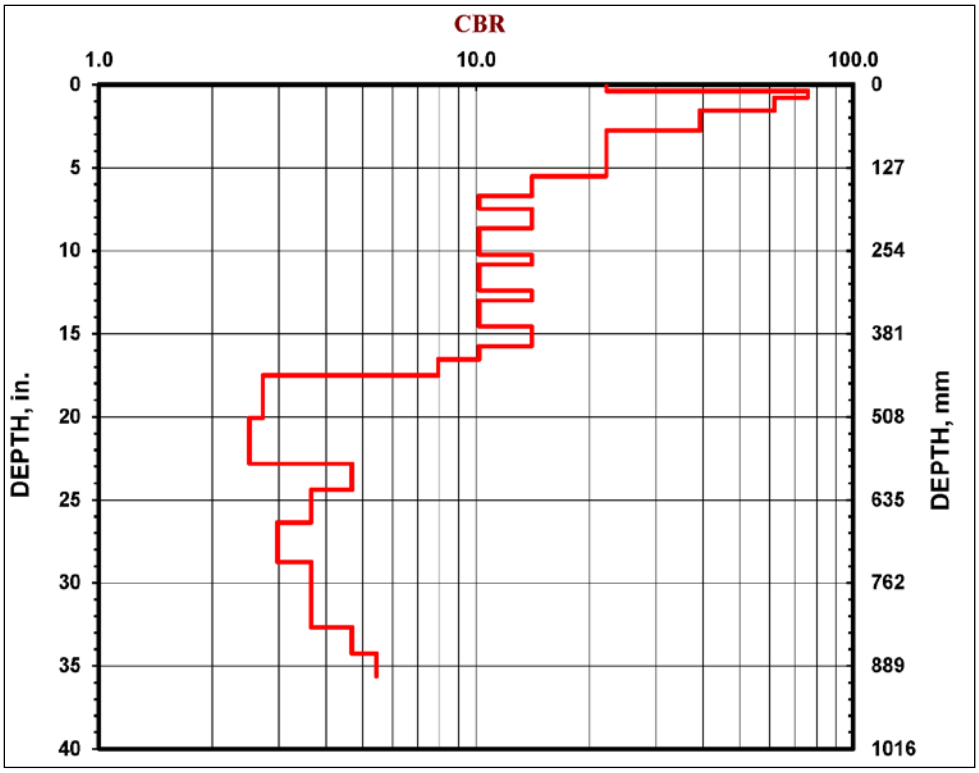

Figure 23. Post-Construction DCP Data Item 1 (Control)

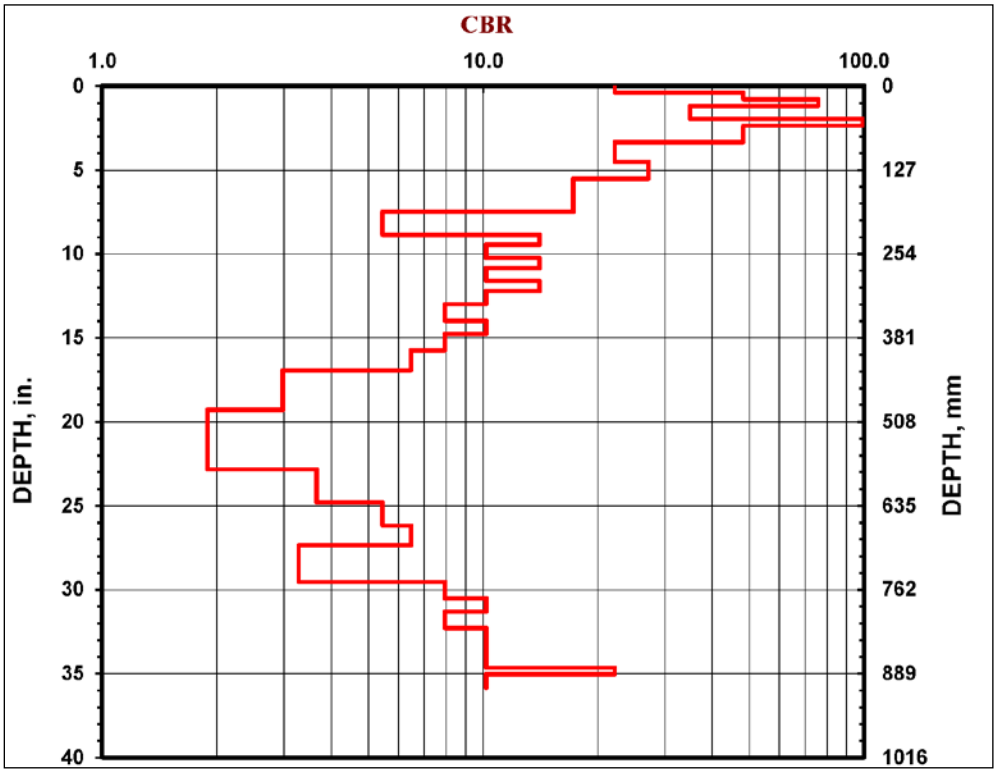

Figure 24. Post-Construction DCP Data Item 2 (TX140)

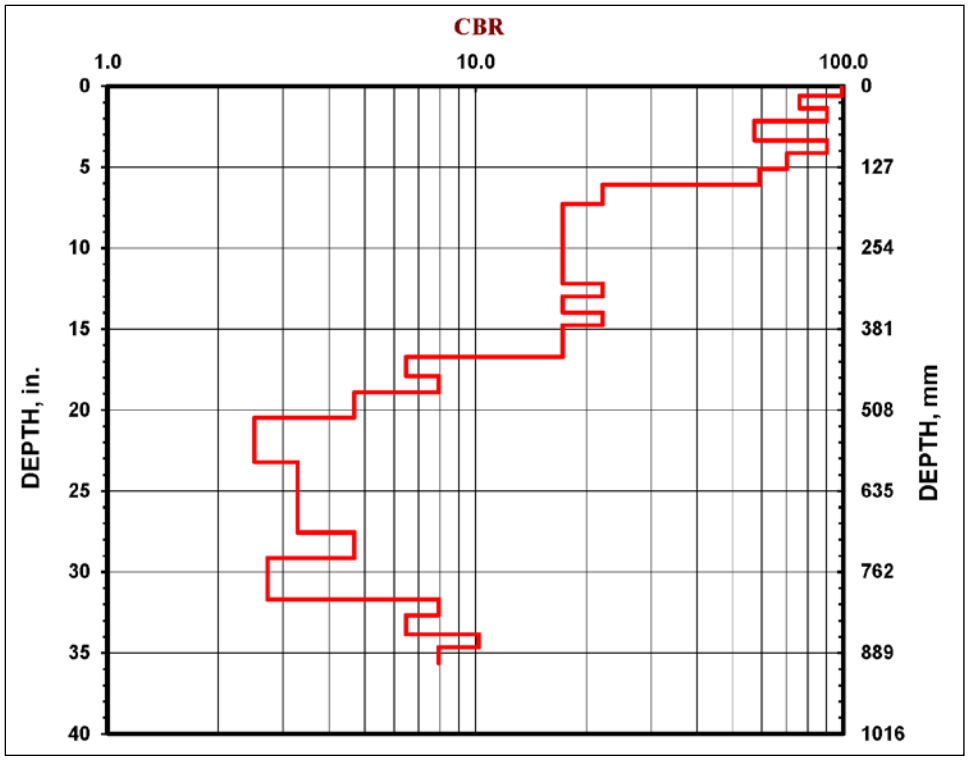

Figure 25. Post-Construction DCP Data Item 3 (BX1200)

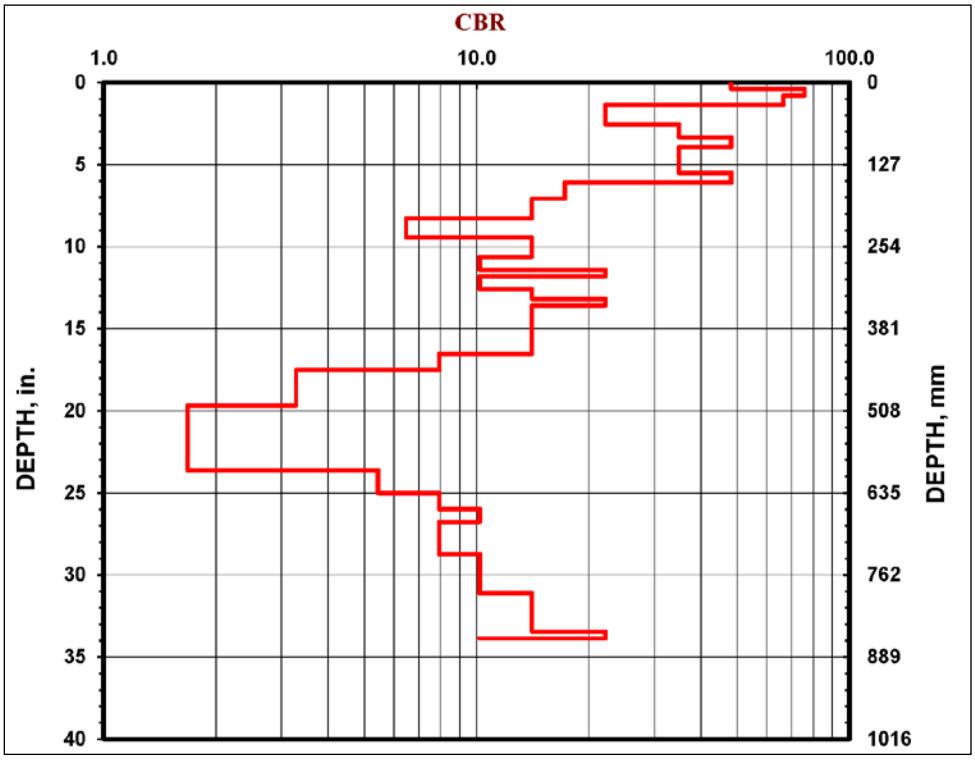

Figure 26. Post-Construction DCP Data Item 4 (Fornit 30/30)

Table 10. The CBR Values of Constructed Layers

Test	Subgrade Surface CBR (%)*	Subbase Surface CBR (%)**	Base-Course Surface CBR (%)*
Control	3.6	15	88
TX140	3.4	15	100+
BX1200	3.2	18	100+
Fornit 30/30	3.1	15	100+

* Determined by ASTM D4429 [8]
** Determined from DCP results

4.6 SURFACE LAYER—HMA.

The asphalt concrete layer used for this project was a locally available dense-graded HMA that met the design requirements for an MDOT HT 12.5-mm mixture with a PG 67-22 binder. To reduce variability in the placement of the HMA in the test box, the HMA was placed in a 12- by 100-ft HMA section and subsequently cut into 5.5-ft-square slabs to be placed in the testing box. The HMA was placed in two lifts; the first lift was 3 in., and the second lift was 2 in. making a final nominal thickness of 5 in. A unique construction method was used to facilitate the movement of the HMA slabs after placement. To transport the HMA slabs to the testing box, the HMA was constructed over 1.5 in. of plywood, as shown in figure 27.

Figure 27. Initial HMA Placement

Upon compaction of the final lift, cores were taken to evaluate the placed HMA properties, as shown in figure 28. Laboratory tests were run on each of the cores as well as samples taking from the paver during construction. The laboratory test results are summarized in table 11 and the field core densities are summarized in table 12. As previously stated, the section was cut into 12 separate 5.5- by 5.5-ft slabs. Each slab was then moved to a covered storage facility to minimize oxidation effects on the HMA, as shown in figures 29 and 30. The HMA slabs were stored under cover for 9 weeks prior to conducting the first box test. This was to let the HMA cure and try to eliminate variability between the test items in HMA stiffness.

Figure 28. Coring of Placed HMA

Table 11. Laboratory HMA Test Results

HMA Volumetric Properties	
Air Voids	3.39
Voids in Mineral Aggregate (VMA) %	13
Voids Filled with Asphalt (VFA) %	89
Theoretical Maximum Specific Gravity (G_{mm})	2.397
Bulk Specific Gravity (G_{mb})	2.313
Bulk (dry) Specific Gravity (G_{sb})	2.52
Unit Weight	144.3
Asphalt Content % (%AC)	5.2

Table 12. The HMA Field Core Densities

Field Core	Unit Weight (pcf)
1	137.1
2	136.2
3	137.1
4	137.0
5	135.9
6	135.3
Average	136.4

Figure 29. The HMA 5.5- by 5.5-ft Slab

Figure 30. Storage of HMA Slabs Prior to Testing

The individual slabs were placed as the surface layer for each induvial test by use of a telehandler. The slabs were brought from storage to the testing box, and the HMA was carefully moved from the plywood to the testing box and placed on top of the base course, as shown in figure 31. Survey readings were taken to get final overall thicknesses of each test section. Also, initial baseline surface deformation readings were taken. Figure 32 shows a test item fully constructed prior to testing.

Figure 31. Placement of HMA on Top of Base Course

Figure 32. Constructed Test Item Prior to Testing

4.7 INSTRUMENTATION.

Sensors were placed in the subgrade, subbase and at the pavement surface to quantify the response of each test item to the loading. The instrumentation layout in profile was shown previously in figure 9. Figure 33 shows the plan view of the surface sensors, and subsurface sensors are shown in figure 34. These sensors are described in greater detail in sections 4.7.1 and 4.7.2.

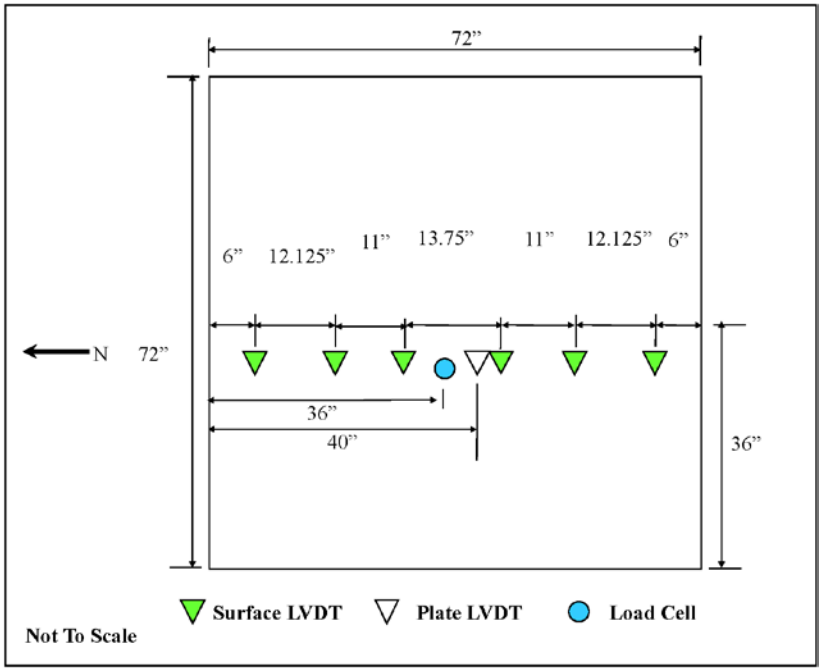

Figure 33. Surface Instrumentation, Plan View

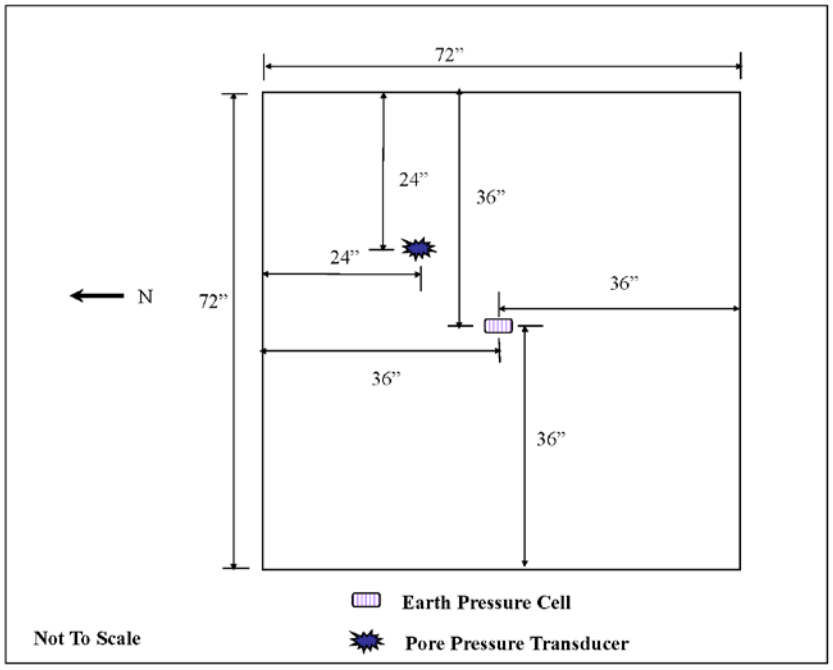

Figure 34. Subbase Instrumentation, Plan View

4.7.1 Subgrade/Subbase.

Two 9-in.-diameter Geokon® Model 3500 EPCs were placed in the subgrade. These sensors were capable of measuring earth pressures up 58 psi. The upper EPC was placed approximately 1 in. below the subbase-subgrade interface, and the lower EPC was placed approximately 2 in. above the bottom of the test section. Both EPCs were placed directly under the center of the loading plate.

After compaction of the lift associated with each EPC, the subgrade was excavated by hand to place the EPC. Soils were carefully removed to ensure that the EPC was placed at the desired depth within the pavement profile. A thin lift of sand was placed beneath the EPC to ensure adequate contact between the bottom of the EPC and the clay subgrade as well as make certain the EPC was level. The clay surface was hand tamped as it was replaced to prevent the inclusion of voids. The subgrade surface was recompacted using the pneumatic hammer in the zone surrounding the EPC prior to placement of the subsequent lift. The elevation of the EPC surface was obtained prior to being recovered with soil, figure 35. The embedment depths of the installed EPCs are summarized in table 13.

Figure 35. Determining Elevation of Installed EPC

Table 13. The EPC Installed Depths

Test Item	Layer		Depth From Interface (in.)	Depth From Surface (in.)
Control	Subgrade	Bottom	25.8	49.8
		Top	1.44	25.44
	Subbase		0.24	11.88
TX140	Subgrade	Bottom	25.92	49.32
		Top	0.84	24.24
	Subbase		0.72	11.64
BX1200	Subgrade	Bottom	25.8	49.68
		Top	0.6	24.48
	Subbase		0.72	12.36
Fornit 30/30	Subgrade	Bottom	25.68	49.8
		Top	0.96	25.08
	Subbase		0.72	12.6

A Geokon® Model 4500S pore pressure transducer was placed 2 in. below the subbase-subgrade interface. This sensor was capable of measuring pore pressures up 50.8 psi. Prior to placement in each test item, the pore pressure sensor was fully saturated. The subgrade was hand excavated

in a manner similar to that used to place the EPCs. The pore pressure sensor was placed in direct contact with the clay subgrade as recommended by the manufacturer. The subgrade was replaced and recompacted prior to placement of the overlying layers.

One Geokon® Model 3500 EPC was installed approximately 1 in. below the interface of the subbase and base course. This EPC was also a Geokon® 9-in.-diameter EPC, but the subbase EPC was capable of accurately reading up 87 psi. The same installation procedures from the subgrade installation were used for the subbase EPC installation. Installation depths are summarized in table 13.

4.7.2 Surface.

Six LVDTs were placed at the surface of the HMA layer. The sensor offsets relative to the center of the loading foot are shown in figure 33. These sensors were placed along the centerline of the pavement surface, providing a mechanism for measuring deflection basins during cyclic plate load testing as well as quantifying the accumulation of permanent deformations at the HMA surface throughout the pavement life. An LVDT was placed on the circular load plate, providing a measure of deformations directly beneath the load. The LVDT setup is shown in figure 36. An additional LVDT is located in the actuator assembly.

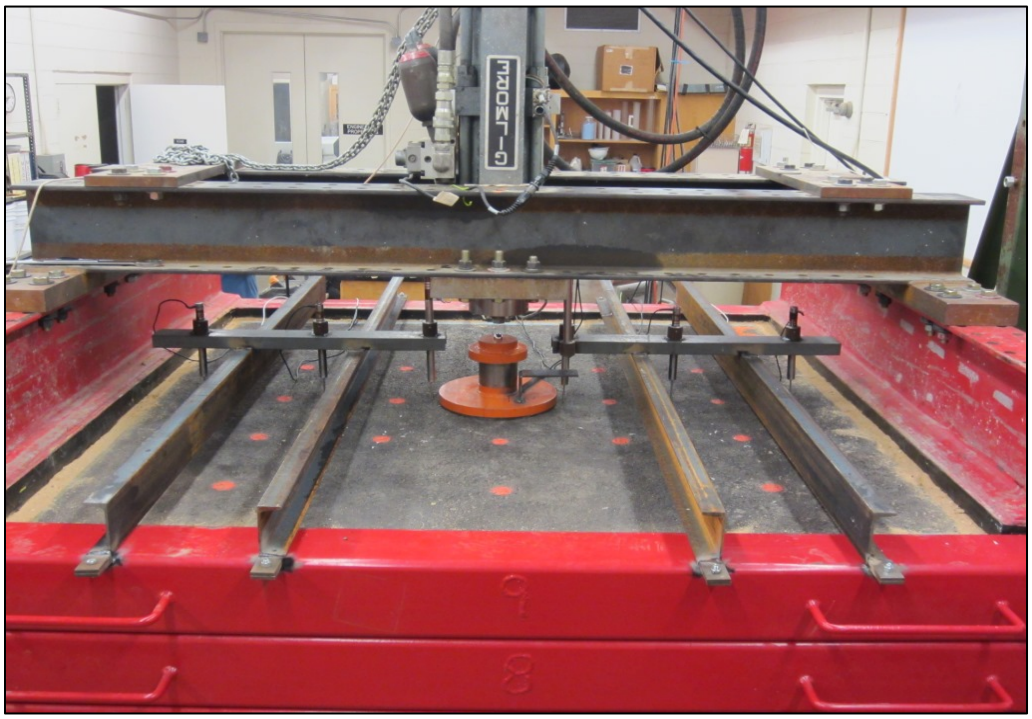

Figure 36. The LVDT Setup on HMA Surface

5. CYCLIC PLATE LOAD TESTING.

Cyclic plate testing was conducted in an attempt to quantify the benefit of geogrid-reinforced airfield pavements. Four test items were subjected to cyclic loading using a hydraulic actuator

and loading plate to a predetermined load that is representative of a typical, heavy FAA aircraft. Section 5.1 discusses the testing procedure in detail.

5.1 TESTING PROCEDURE.

The testing system consisted of a 50,000-lb hydraulic actuator used to apply cyclic loads to the pavement test items. Testing was controlled using a computerized MTS Systems® control system. The load was transmitted to the pavement via a 12-in.-diameter, 1-in.-thick steel plate. Attached to the bottom of the steel plate was a 0.25-in.-thick neoprene pad to reduce stress concentrations near the edge of the load plate. Applied loads were measured using a load cell located between the actuator and the load plate. The load cell used in this experiment had a capacity of 50,000 lb, as shown in figure 37.

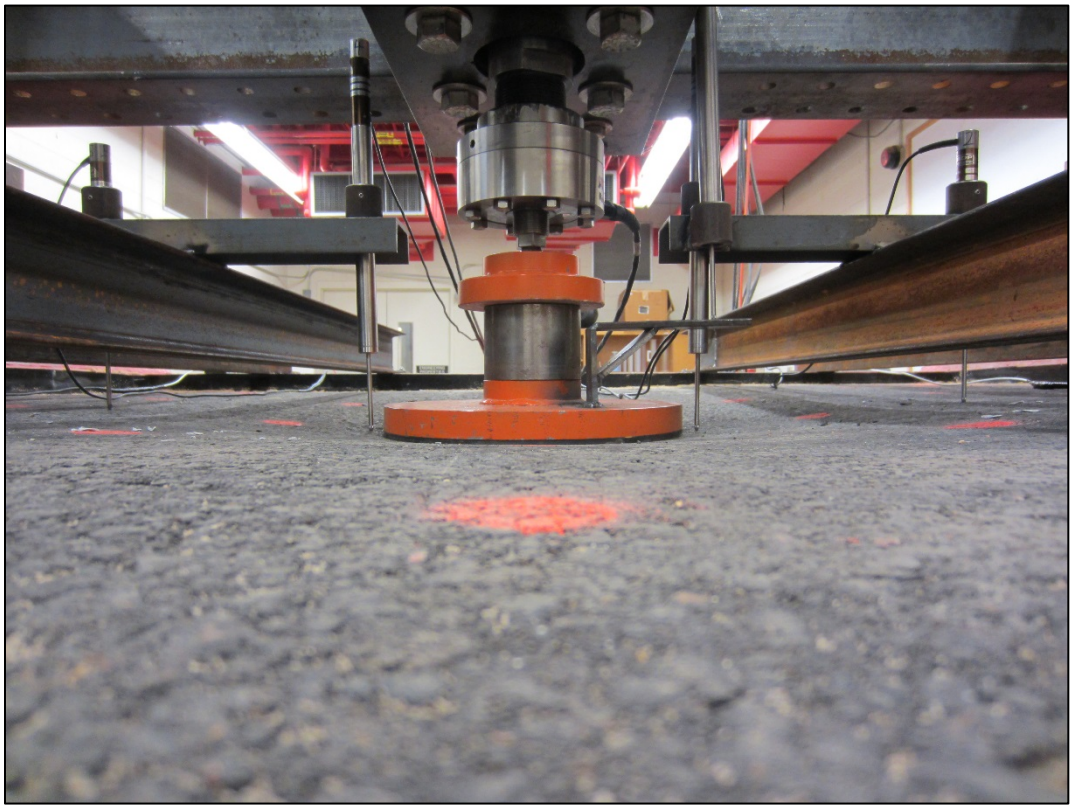

Figure 37. The 50,000-lb Load Cell Setup

Each load pulse was applied with a total duration of 1.2 seconds. The load was applied for a 0.3-second duration followed by a 0.9-second rest period. Each test item was loaded using a target load of 28,800 lb applied to a 12-in.-diameter plate to achieve a 254.6-psi load applied to the HMA surface. During the rest period, a 100-lb surcharge was maintained. A typical set of load pulses is displayed in figure 38.

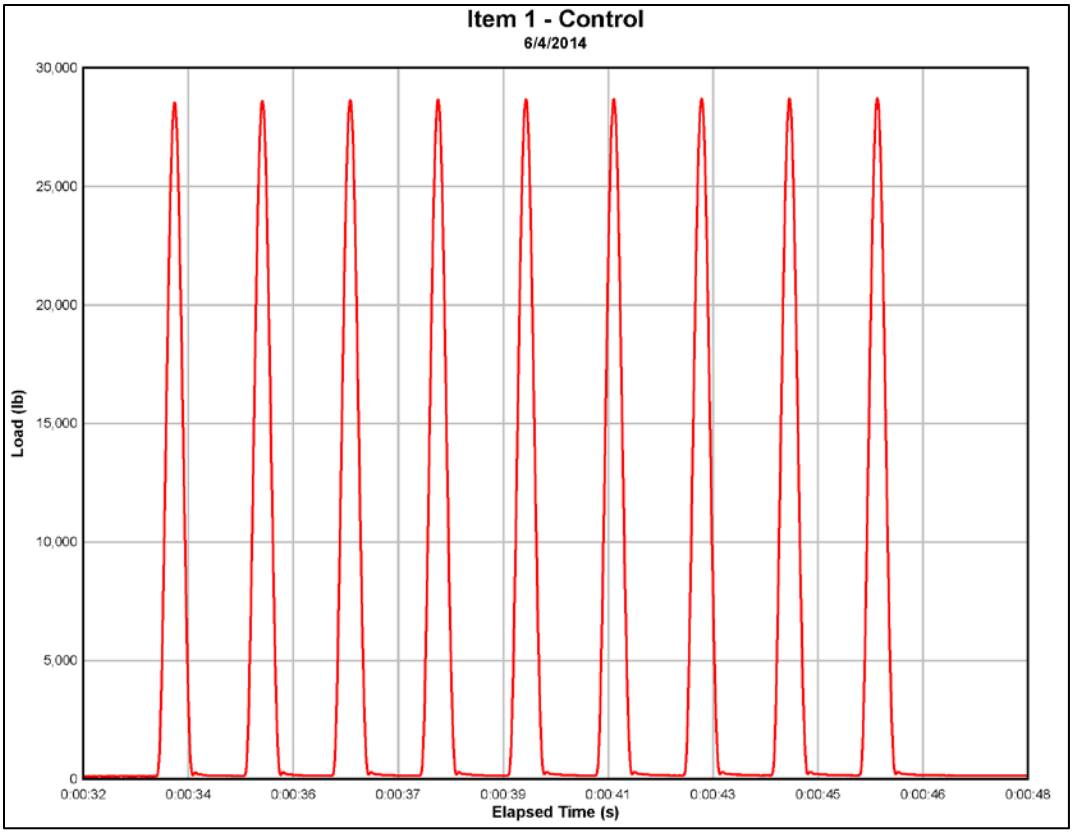

Figure 38. Sinusoidal Applied Load Pulses for a Typical Test

Testing proceeded in the following manner. The 28,800-lb load was applied to the center of the HMA surface. Instrumentation response data for the LVDTs, EPCs, and load cell were constantly recorded at a rate of 500 Hz. Dynamic and permanent surface deformations were constantly monitored. Testing was periodically halted to monitor permanent deformation after a brief resting period. Video recordings of every pulse sequence for each test item were taken. Testing was concluded after permanent deformation for each test item was greater than 2 in.

5.2 RESULTS.

Table 14 presents the load level required for each test item to reach 2 in. of permanent surface deformation. As defined in AASHTO Designation R50-09 [3], the TBR is defined as the ratio of the number of load cycles of a reinforced pavement to reach a defined failure state, to the number of loads for the same unreinforced section to reach the same defined failure state. Two separate TBR values were calculated based on the load levels required to produce 1- and 2-in. permanent deformations in the surface of the test items. A summary of the TBR values is also presented in table 14. It should be noted that the TX140 test item only had a 6-in. base course compared to all the other items that had approximately 7-in. base-course thicknesses. Therefore, it is prudent to compare the TX140 to the control item but not the other geogrid-reinforced items. The permanent deformations measured at the plate for all items tested are graphically shown in figure 39.

Table 14. Load Cycles to Failure and TBR

Product	Load Level at 1-in. Permanent Deformation	Load Level at 2-in. Permanent Deformation	TBR at 1-in. Permanent Deformation	TBR at 2-in. Permanent Deformation
Control	304	1,278	-	-
TX140*	1,000	4,304	3.3	3.4
BX1200	6,322	25,960	20.8	20.3
Fornit 30/30	9,024	34,901	29.7	27.3

* Note: The TX140 only had a 6-in. base course.

The response from the EPCs installed in the bottom of the subgrade layer is presented in figure 40. EPC readings from the top of the subgrade are shown in figure 41. Responses from the EPC installed in the top of the subbase layer are displayed in figure 42.

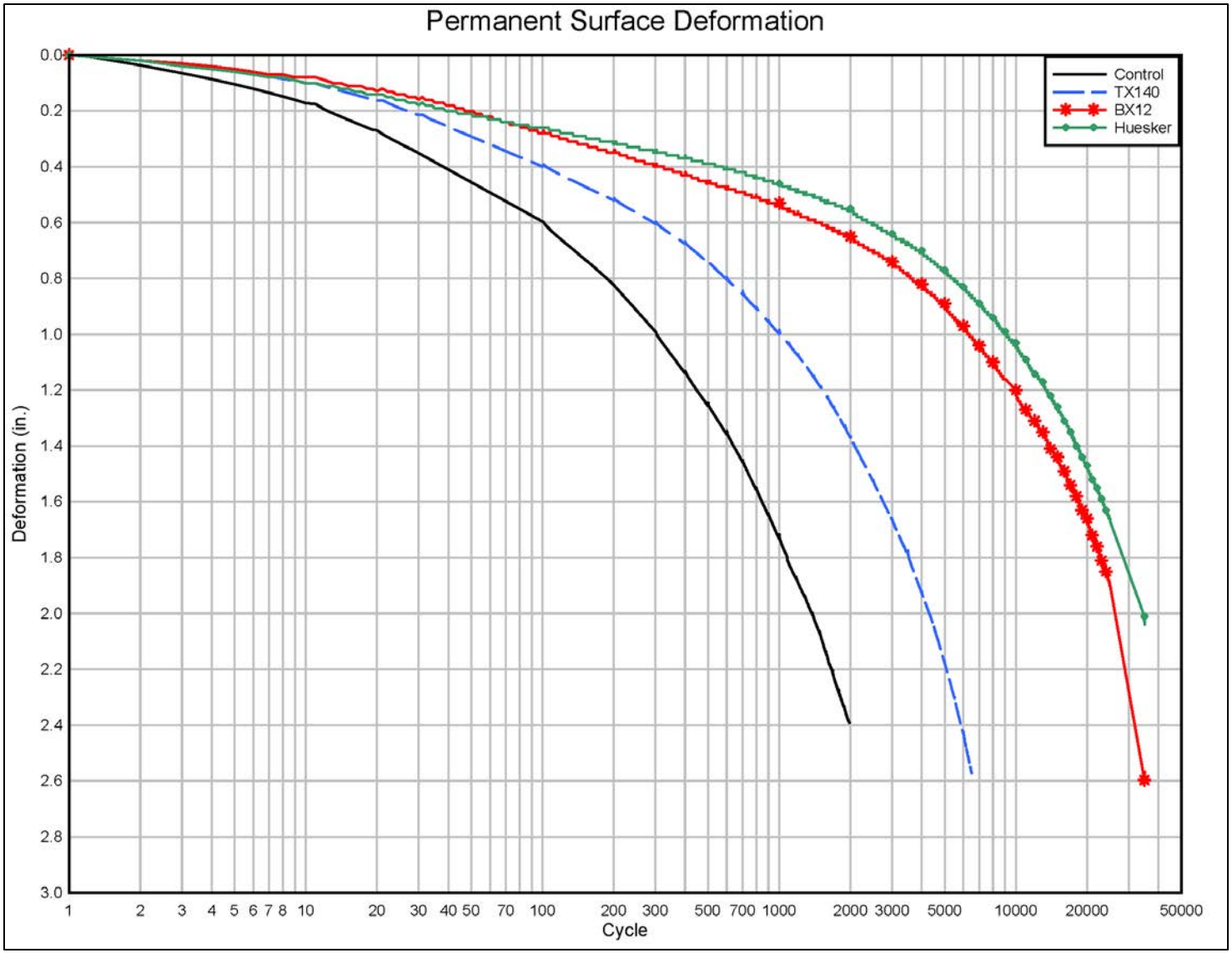

Figure 39. Permanent Surface Deformation

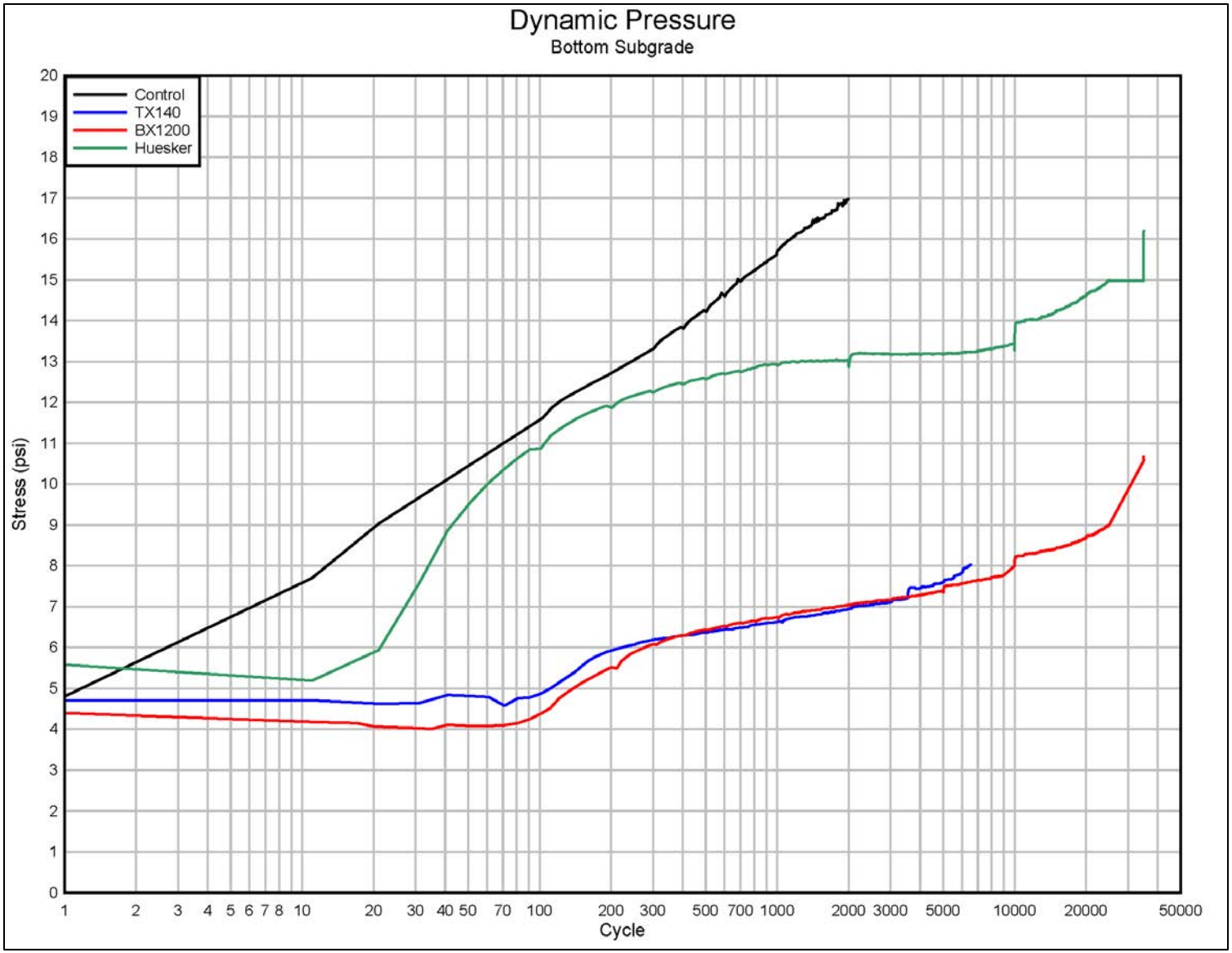

Figure 40. The EPC Response in the Bottom of the Subgrade

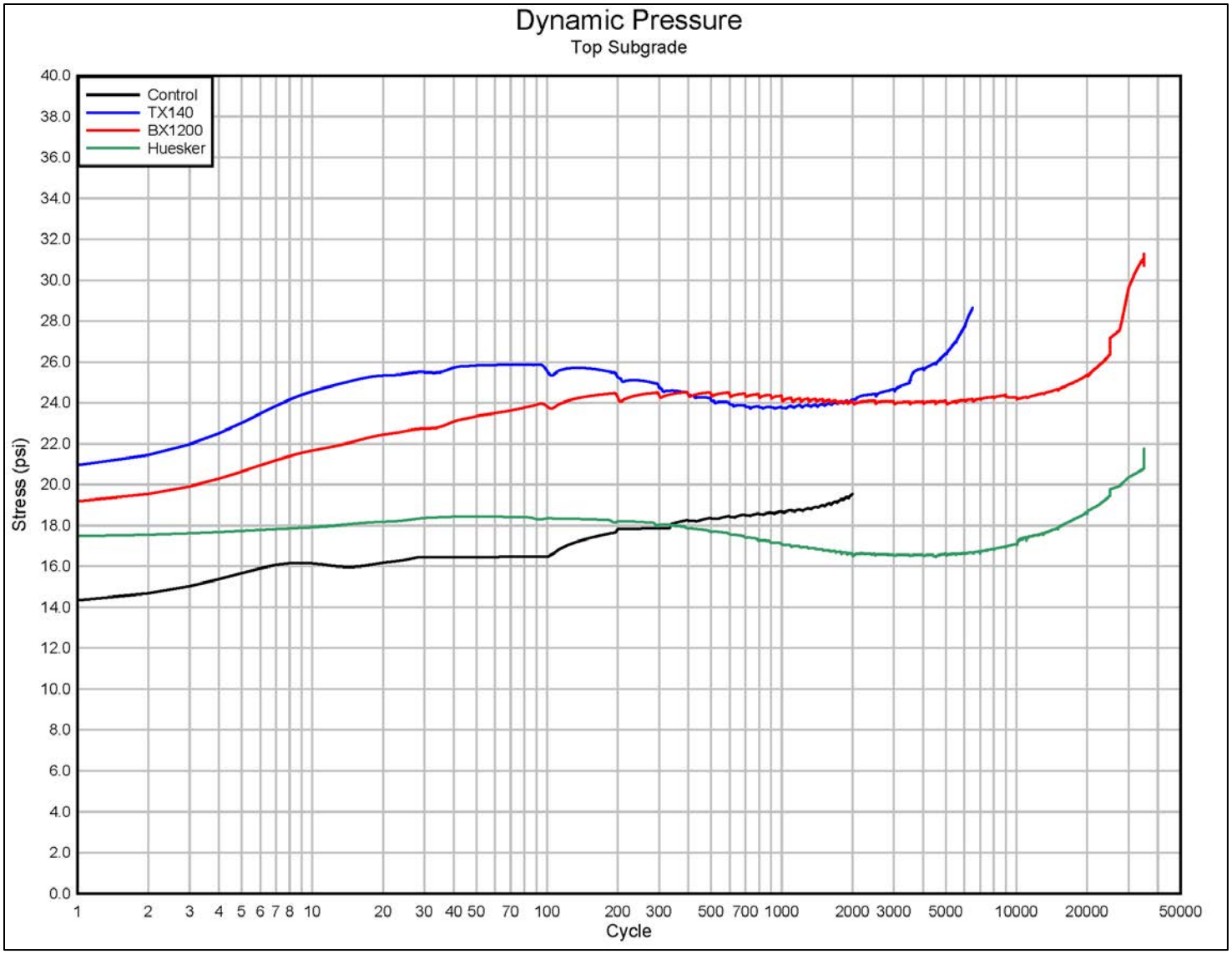

Figure 41. The EPC Response in the Top of the Subgrade

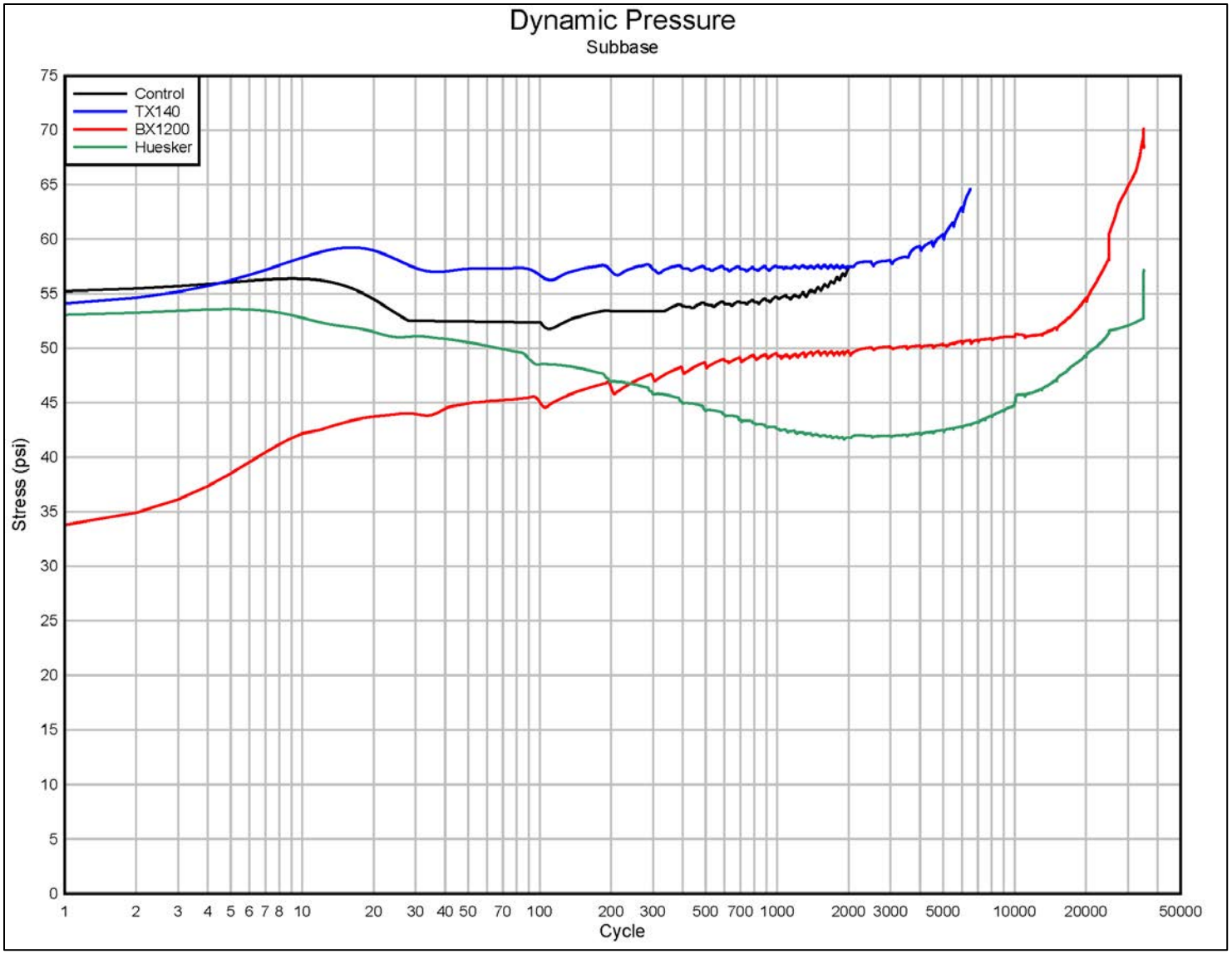

Figure 42. The EPC Response in the Subbase

5.3 POST-TEST FORENSICS.

After each item was tested individually, a series of tests were performed to quantify any changes in physical properties during the initial testing to quantify the strength of the pavement layers and the deformations associated with testing. Readings were taken for the HMA surface, base-course surface, subbase surface, and the subgrade surface.

After an item was tested, the HMA surface was surveyed to quantify the permanent surface deformation that occurred. Rut depth measurements were taken across the centerline of the HMA surface as well. Figure 43 presents the photos of the rut depth measurements on the HMA surface for each test item. The HMA layer was then saw-cut down the centerline of the surface. The front half of the HMA was carefully removed to expose the base-course surface. Survey and rut depth readings were taken on the exposed surface of base course. Figure 44 shows the excavated base-course surface photos from each test item. The base course was then saw-cut down the centerline and carefully removed to expose the subbase surface. Survey and rut depth readings were taken on the surface of the subbase, as shown in figure 45. The subbase layer was removed to expose the surface of the subgrade. Survey and rut depth measurements were also taken at the subgrade surface, as shown in figure 46. Summary plots of the permanent layer deformations are shown in figures 47 through 50. It should be noted that each test item was subjected to a different number of loadings. Therefore, the deformation plots should be used to demonstrate the lack of deformation in the subgrade layers of the geogrid-reinforced items versus the amount of deformation experienced in the unreinforced control item. For comparison purposes, the number of loadings at 2-in. permanent HMA surface deformation was previously reported in table 14.

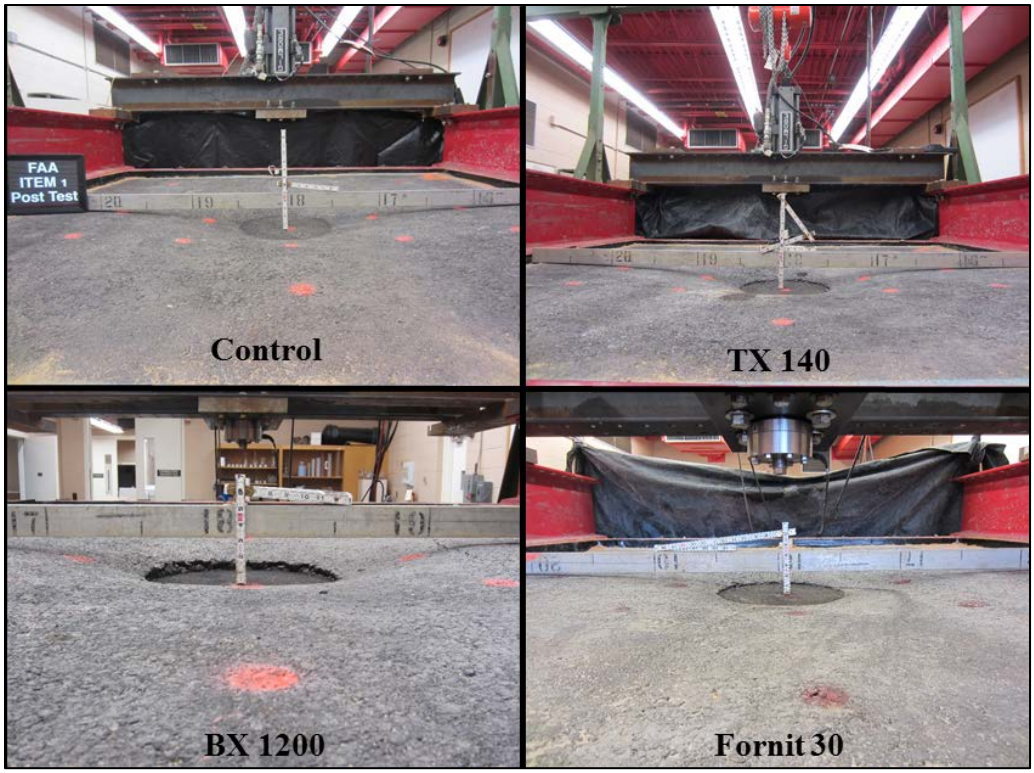

Figure 43. Post-Test Rut Depth Measurements of the HMA Surface

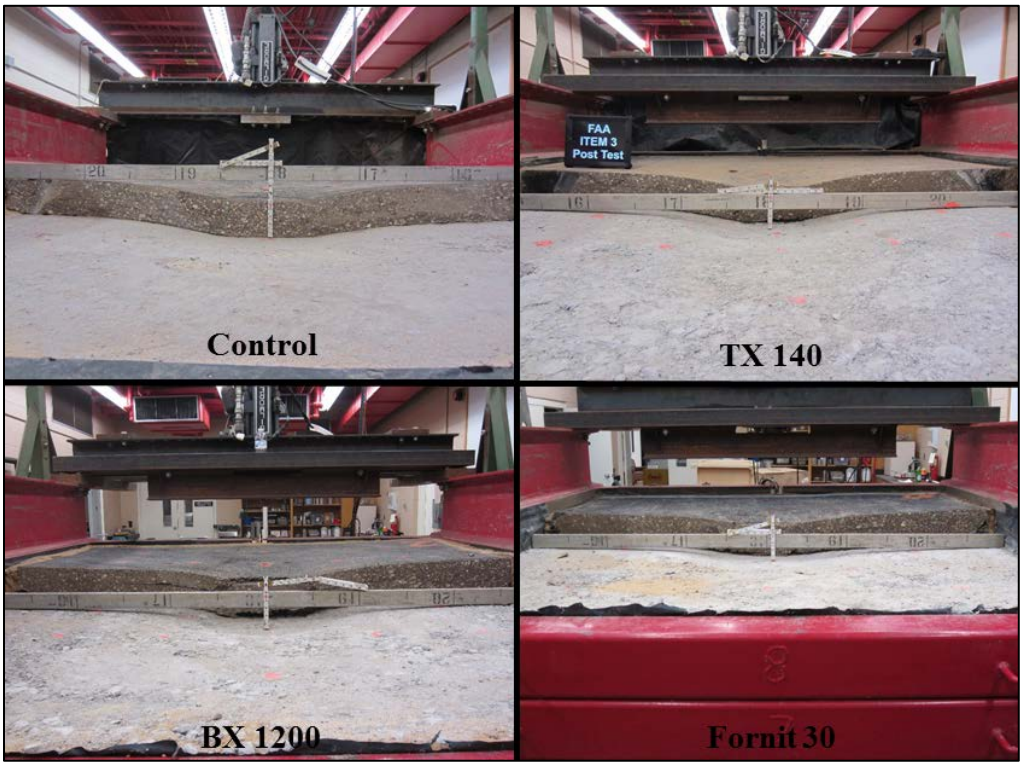

Figure 44. Post-Test Excavated Base-Course Surface

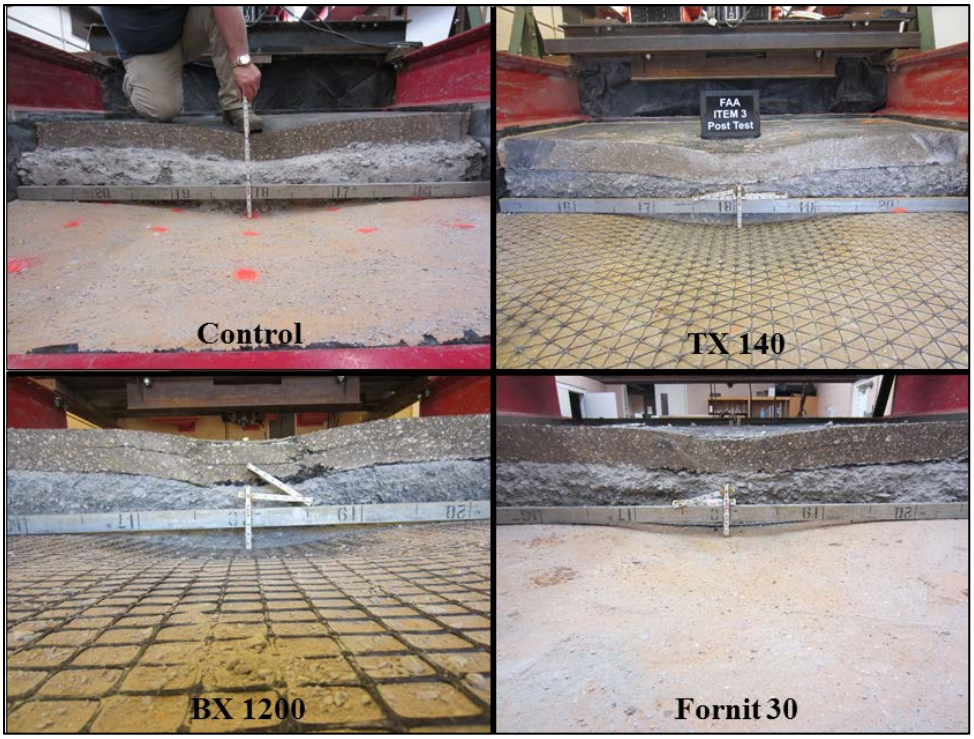

Figure 45. Post-Test Excavated Subbase Surface

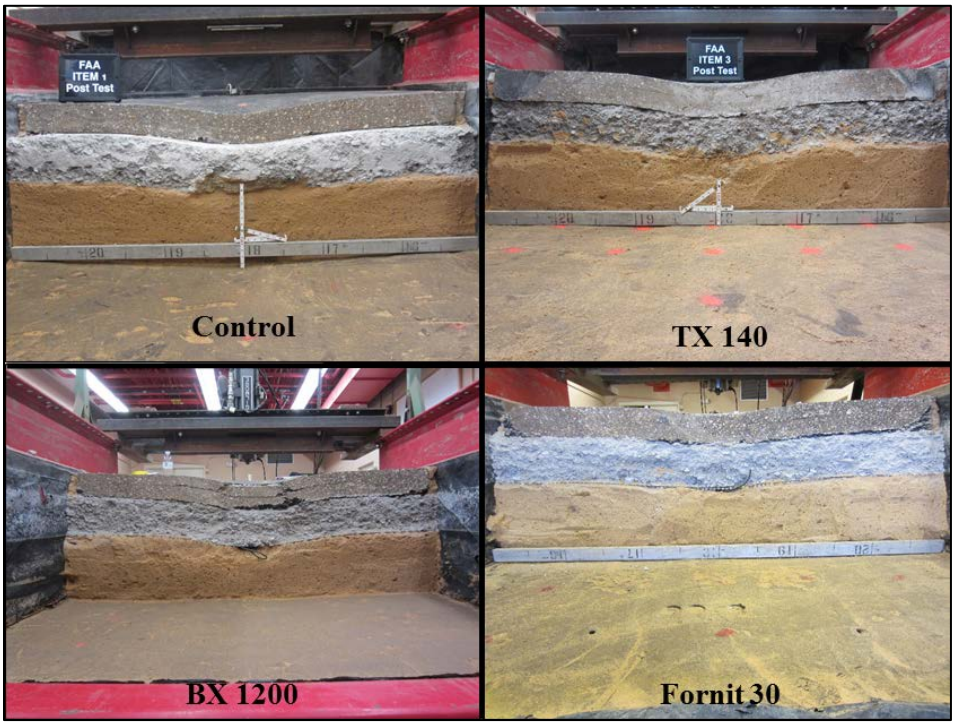

Figure 46. Post-Test Excavated Subgrade Surface

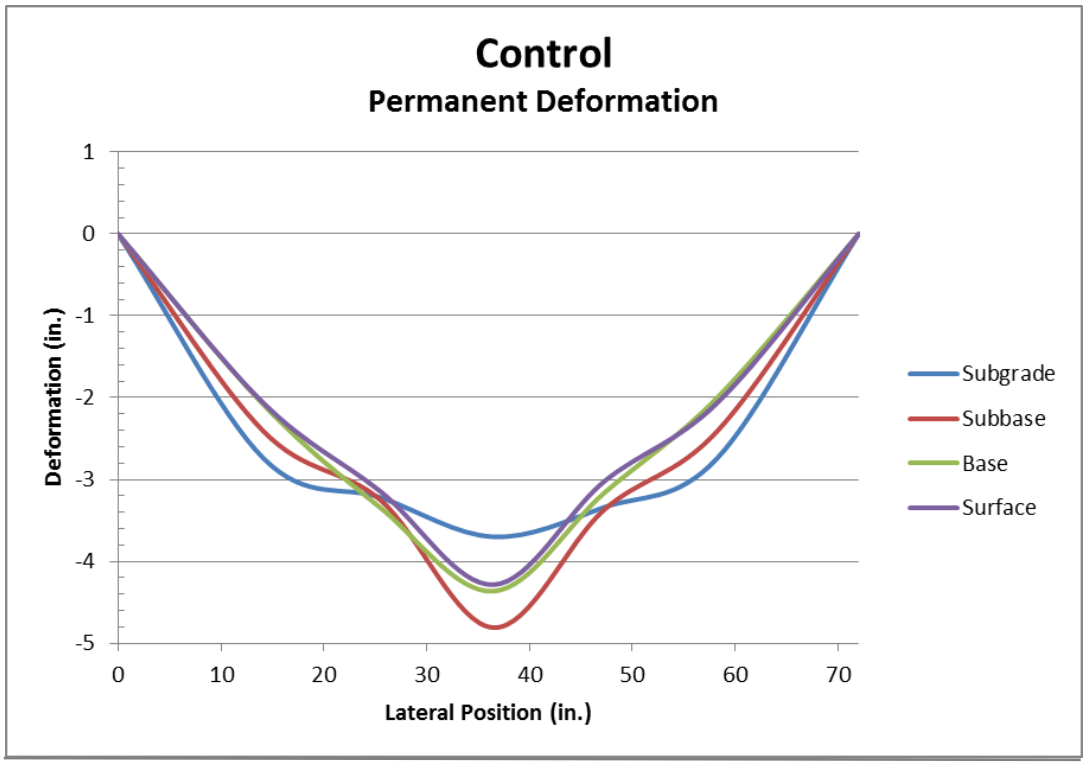

Figure 47. Permanent Layer Deformations for the Control

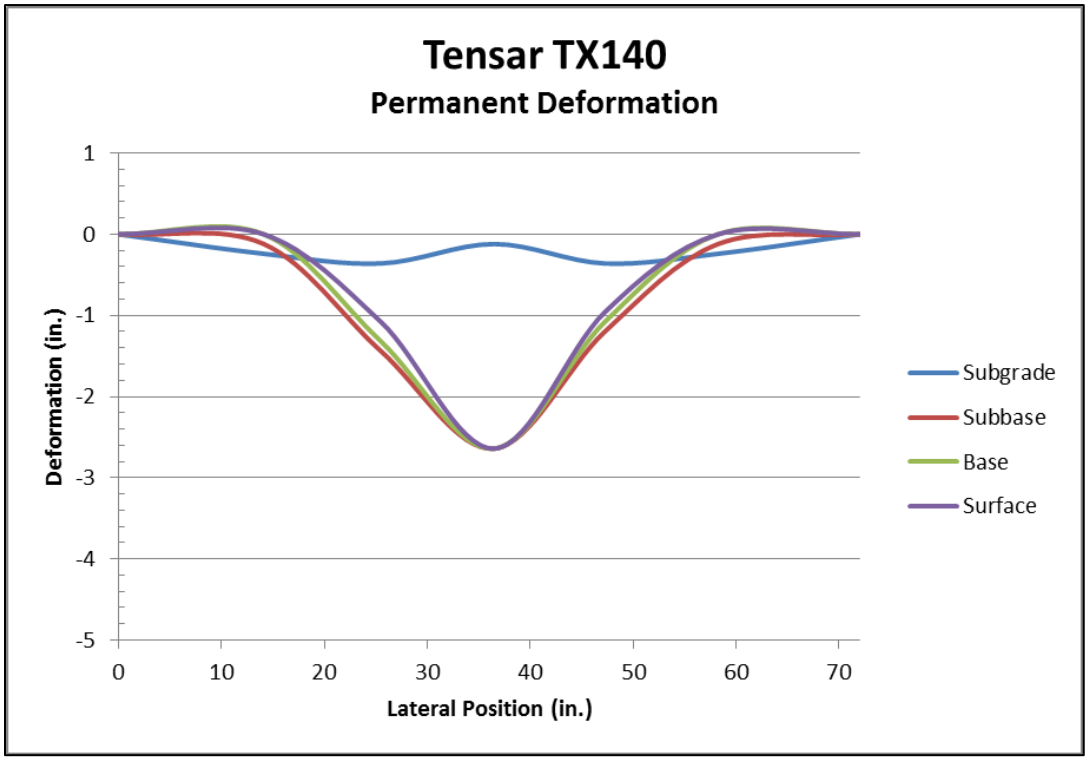

Figure 48. Permanent Layer Deformations for TX140

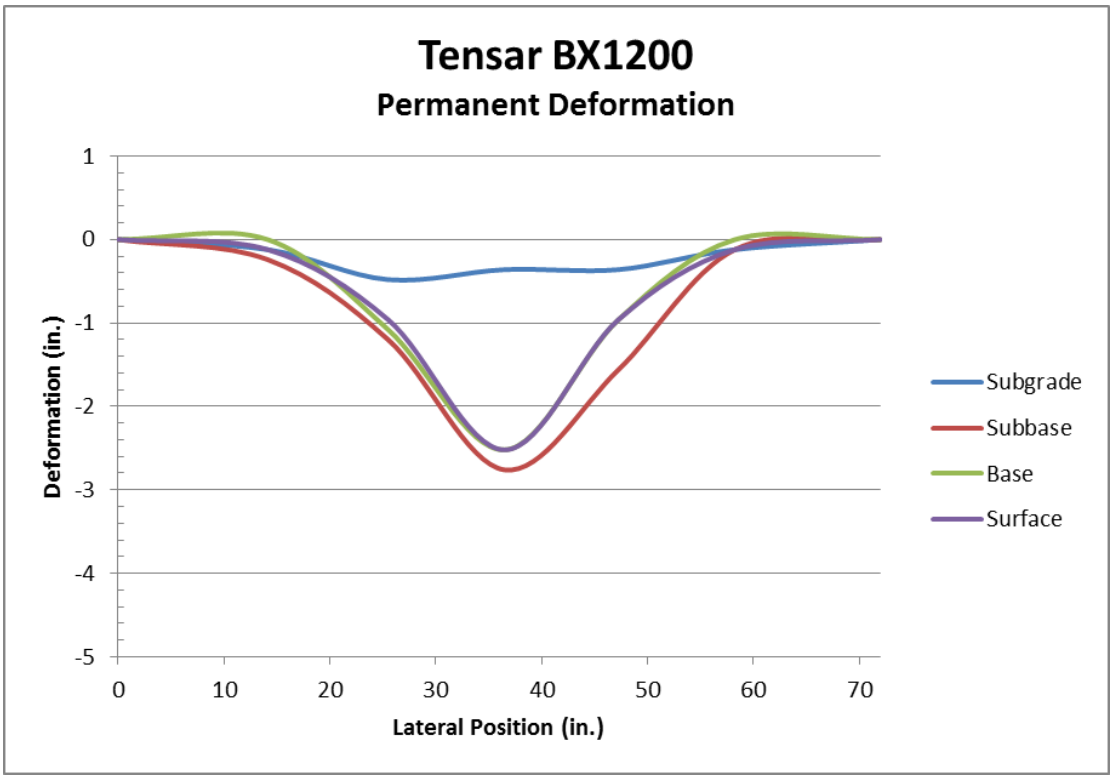

Figure 49. Permanent Layer Deformations for BX1200

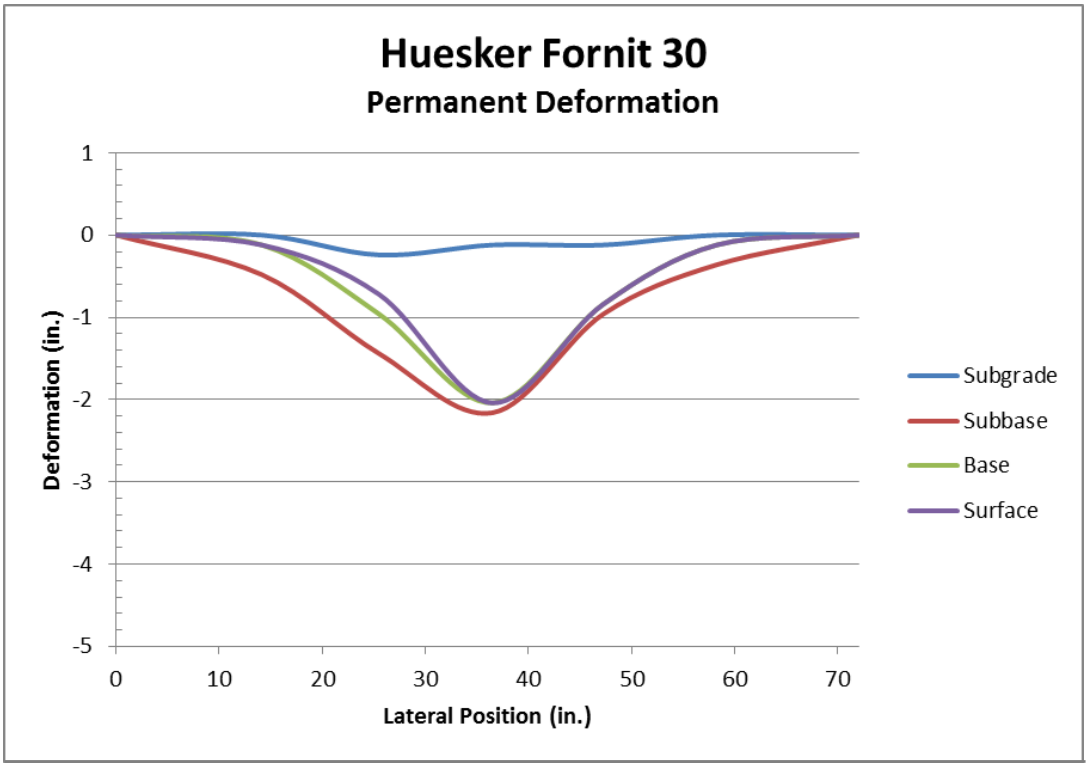

Figure 50. Permanent Layer Deformations for Fornit 30/30

Post-test strength characteristics were obtained through DCP tests and field in-place CBR tests for each test item. The DCP plots are displayed in figures 51 through 54. The DCP tests for each item were conducted outside of the damaged area and were used to determine if the underlying layers changed significantly during testing. The results from the post-test DCP tests demonstrate the test items underwent virtually no change during testing. The only noticeable change was a slight increase in strength in the HUESKER Fornit 30/30 subgrade. Field in-place CBR test were conducted on the excavated base and subgrade surfaces. The tests were conducted inside the rut, which is the permanently deformed area directly under the applied load as well as outside of the damaged area. For the geogrid-reinforced items, there was no permanent deformation in the subgrade layer, so only one set of tests were conducted for those items. Results from the post-test field in-place CBR tests are summarized in table 15. Results indicate the test items lost significant strength in the base course directly under the loading plate due to failure and permanent deformation of the pavement structure.

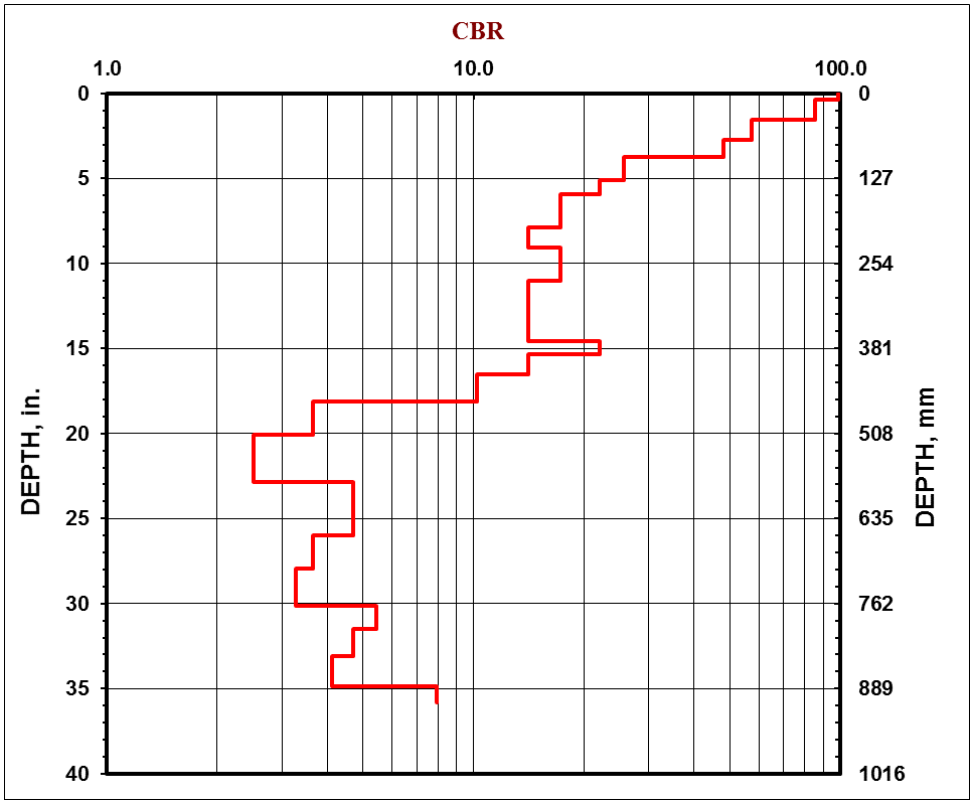

Figure 51. Post-Test DCP for Control

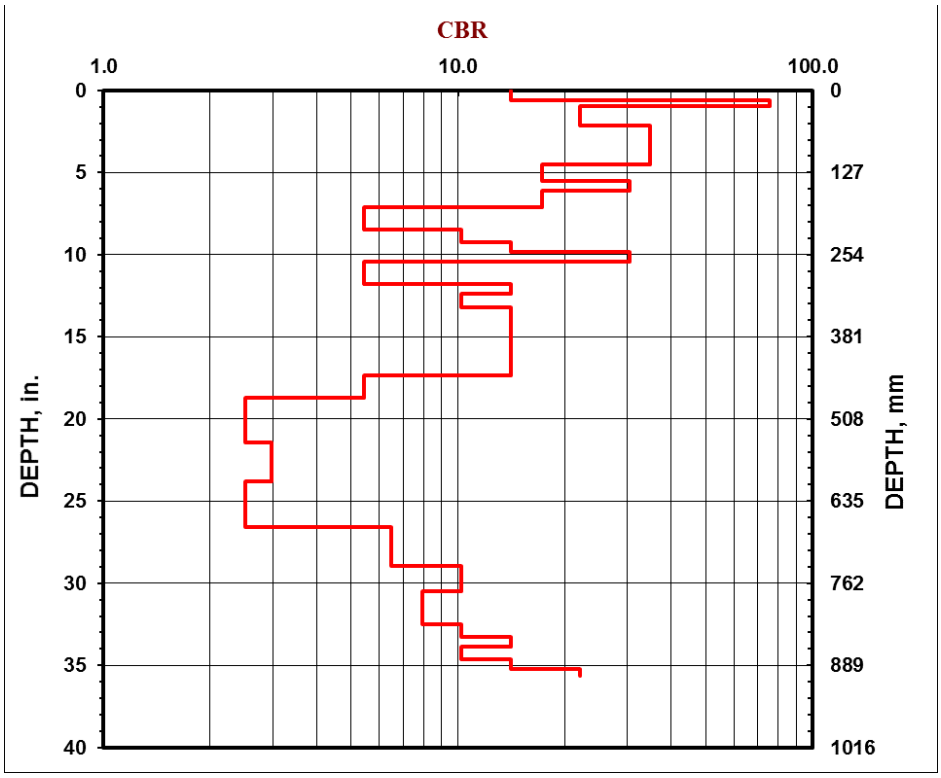

Figure 52. Post-Test DCP for TX140

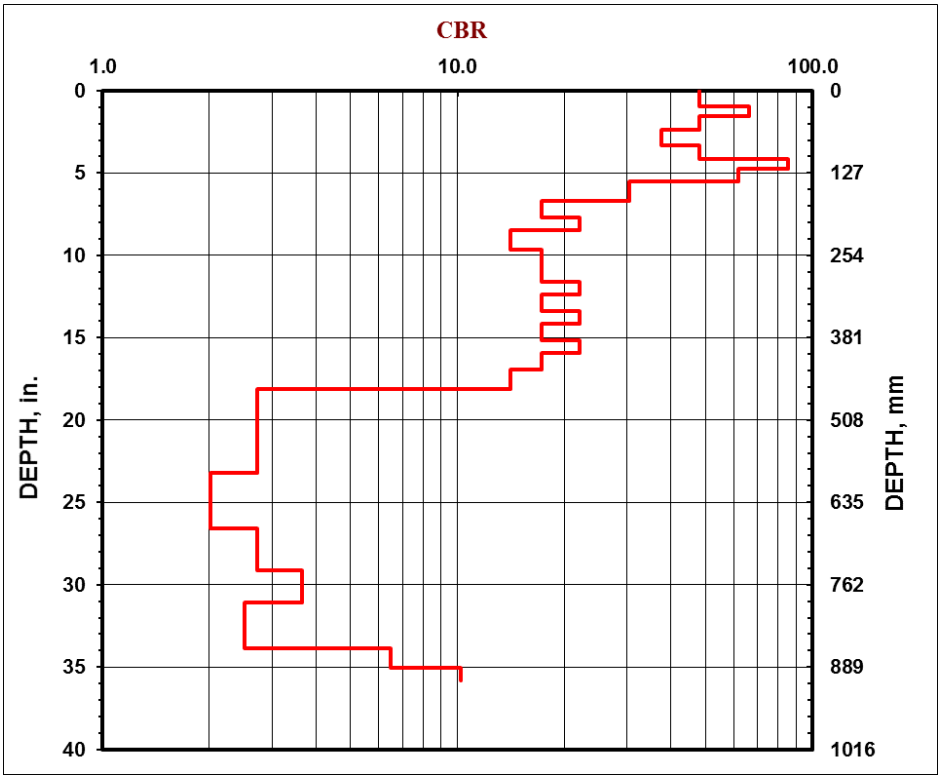

Figure 53. Post-Test DCP for BX1200

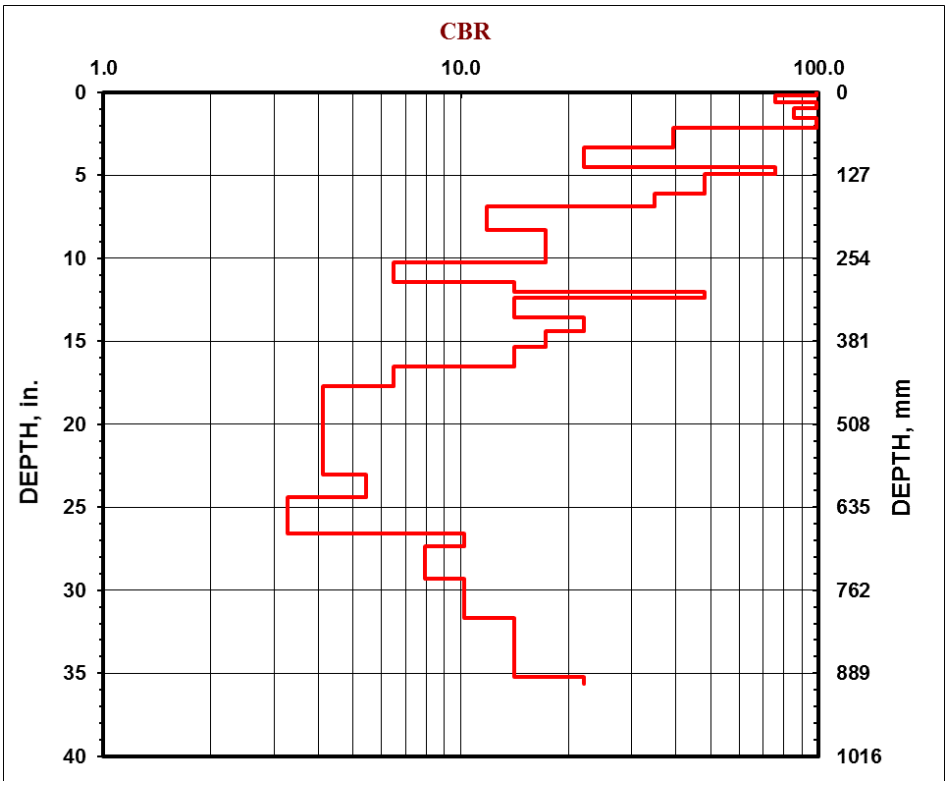

Figure 54. Post-Test DCP for Fornit 30/30

Table 15. Summary of Post-Test Field In-Place CBR Values

Test	Subgrade Surface CBR (%) In Rut	Subgrade Surface CBR (%) Out of Rut	Base Surface CBR (%) In Rut	Base Surface CBR (%) Out of Rut
Control	4.1	3.2	64	76.0
TX140	2.5	NA	48	66.0
BX1200	3.6	NA	44	91.5
Fornit 30/30	3.7	NA	54	97.5

Post-test measurements of density and moisture content were obtained for each layer using the nuclear densometer. These tests were conducted outside of the damaged areas of each item. Results are summarized in table 16. As shown from the results in table 15, there were no discernable changes to density or moisture. Only the TX140 test item exhibited an evident change, which occurred in the base course. There was a 13-pcf drop in dry density of the base course from the pretest data collection.

Table 16. Post-Test Density and Moisture Data

Product	Layer	Wet Density (pcf)	Dry Density (pcf)	Moisture Content (%)
Control	Subgrade	110.5	82.7	33.6
	Subbase	111.4	109.5	1.8
	Base	137.2	135.4	1.4
TX140	Subgrade	111.2	82.9	34.2
	Subbase	111.9	110.3	2.8
	Base	127.7	124.9	2.0
BX1200	Subgrade	108.7	81.4	33.6
	Subbase	110.6	107.7	2.7
	Base	135.6	132.6	2.3
Fornit 30/30	Subgrade	114.8	88.4	29.9
	Subbase	110.0	108.5	1.4
	Base	138.5	136.5	1.5

6. CONCLUSIONS AND RECOMMENDATIONS.

The ERDC tested and evaluated four test items, including one unreinforced item and three geogrid-reinforced items. The four test items were constructed in the laboratory box-testing facility with each reinforced item containing a unique geogrid placed at the base/subbase interface. This report addresses the construction and testing procedures of the cyclic plate load testing of the pavement test items. Conclusions and recommendations based on results from the testing are summarized in sections 6.1 and 6.2, respectively.

6.1 CONCLUSIONS.

The following conclusions resulted from the construction and cyclic plate testing:

- Pavement performance greatly improved with the geogrid-reinforced test items compared to the unreinforced control item. The unreinforced control item failed at a lower pass level than any of the geogrid-reinforced items. The traffic benefit ratio (TBR) values for the geogrid-reinforced items with a 7-inch base course ranged from 20.3 to 29.7. The TBR values for the 6-inch base when compared to the 7-inch base unreinforced item were 3.3 and 3.4.

- Subgrade rutting and damage was exhibited in the unreinforced control item, whereas no measureable rutting was present for any of the geogrid-reinforced items.

- With the exception of the 6-inch base course in the TX140 test item, all items were constructed with minimal nonsignificant differences between them. This allows for performance comparisons to be made between the items.

6.2 RECOMMENDATIONS.

Based on the testing conducted, the following recommendations are provided:

- It is recommended that these results be used as a basis for additional full-scale accelerated pavement testing using Federal Aviation Administration aircraft loadings. The increase in TBR for all the geogrid-reinforced test items proves the potential for significant benefits of incorporating geogrid reinforcement into airfield flexible pavement design methodologies. Full-scale accelerated pavement testing could produce different results due to the nature of a rolling wheel load versus a vertically applied cyclic load.

- The performance of the TX140 test item should only be compared to the unreinforced control test item. Due to the difference in constructed base-course thickness the performance of the TX140 geogrid cannot be assumed to be any less effective than the other geogrid products. Additional testing needs to be conducted to glean a meaningful comparison between the geogrid products.

- Additional products, such as high-strength geotextile fabrics and other types of geogrid products that have been proven to be beneficial to pavement performance, should be included in future studies.

7. REFERENCES.

1. ASTM International, "Standard Practice for Classification of Soils for Engineering Purposes (Unified Soil Classification System)," ASTM D2487-11, West Conshohocken, Pennsylvania, May 1, 2011.

2. American Association of State Highway and Transportation Officials (AASHTO), "Standard Specification for Classification of Soils and Soil-Aggregate Mixtures for Highway Construction Purposes," AASHTO M145-91, Washington, D.C., 1991.

3. AASHTO, "Recommended Practice for Geosynthetic Reinforcement of the Aggregate Base Course of Flexible Pavement Structures," AASHTO R 50-09, Washington, D.C., October 2009.

4. American Society for Testing and Materials (ASTM) International, "Standard Test Methods for Laboratory Compaction Characteristics of Soil Using Modified Effort," ASTM D1557-12e1, West Conshohocken, Pennsylvania, May 2012.

5. ASTM International, "Standard Test Methods for Liquid Limit, Plastic Limit, and Plasticity Index of Soils," ASTM D4318-10E1, West Conshohocken, Pennsylvania, January 2010.

6. ASTM International, "Standard Test Method for Determining Tensile Properties of Geogrids by the Single or Multi-Rib Tensile Method," ASTM D6637/D6637M-15, West Conshohocken, Pennsylvania, July 15, 2015.

7. Federal Aviation Administration (FAA), “Standards for Specifying Construction at Airports,” AC 150/5370-10G, July 21, 2014.

8. ASTM International, “Standard Test Method for CBR (California Bearing Ratio) of Soils in Place (Withdrawn 2018),” ASTM D4429-09a, West Conshohocken, Pennsylvania, December 1, 2009 (withdrawn 2018).

9. Webster, S.L., Grau, R.H., and Williams, T.P., “Description and Application of Dual Mass Dynamic Cone Penetrometer,” U.S. Army Corps of Engineers, Instruction Report GL-92-3, Final Report, AD-A251 960, U.S. Army Engineers Waterways Experiment Station, Vicksburg, Mississippi, May 1992.

10. Webster, S.L., Brown, R.W., and Porter, J.R., “Force Projection Site Evaluation Using the Electrical Cone Penetrometer (ECP) and the Dynamic Cone Penetrometer (DCP),” U.S. Army Corps of Engineers, Technical Report GL-94-17, AD-A282 441, U.S. Army Engineers Waterways Experiments Station, Vicksburg, Mississippi, April 1994.